Microtubule dynamics: Caps, catastrophes, and coupled hydrolysis

Henrik Flyvbjerg,[1,2,3,*] Timothy E. Holy,[1] and Stanislas Leibler[1]
[1]*Department of Physics and Department of Molecular Biology, Princeton University, Princeton, New Jersey 08544-708*
[2]*Höchstleistungsrechenzentrum, Forschungszentrum Jülich, D-52425 Jülich, Germany*
[3]*Department of Optics and Fluid Dynamics, Risø National Laboratory, DK-4000 Roskilde, Denmark*
(Received 25 April 1996)

An effective theory is formulated for the dynamics of the guanosine triphosphate (GTP) cap believed to stabilize growing microtubules. The theory provides a ''coarse-grained'' description of the cap's dynamics. ''Microscopic'' details, such as the microtubule lattice structure and the fate of its individual tubulin dimers, are ignored. In this cap model, GTP hydrolysis is assumed to be stochastic and uncoupled to microtubule growth. Different rates of hydrolysis are assumed for GTP in the cap's interior and for GTP at its boundary with hydrolyzed parts of the microtubule. Expectation values and probability distributions relating to available experimental data are derived. Caps are found to be short and the total rate of hydrolysis at a microtubule end is found to be *dynamically* coupled to growth. The so-called *catastrophe rate* is a simple function of the microtubule growth rate and fits experimental data. A constant nonzero catastrophe rate, identical for both microtubule ends, is predicted at large growth rates. The *delay time* for dilution-induced catastrophes is stochastic with a simple distribution that fits the experimental one and, like the experimental one, does not depend on the rate of microtubule growth before dilution. The *GTP content* of microtubules is found and its rate of hydrolysis is determined under the circumstances created in an experiment designed to measure this GTP content. It is concluded that this experiment's failure to register any GTP content is consistent with the model. A recent experimental result for the size of the minimal cap that can stabilize a microtubule is shown to agree with the result predicted by the cap model, after its parameters have been extracted from previous experimental results. Thus the effective theory and cap model presented here provide a unified description of several apparently contradictory experimental data. Experimental results for the catastrophe rate at different concentrations of magnesium ions and of microtubule associated proteins are discussed in terms of the model. Feasible experiments are suggested that can provide decisive tests of the model and determine its three parameters with higher precision. [S1063-651X(96)09810-8]

PACS number(s): 87.10.+e, 05.40.+j, 87.22.Bt, 82.35.+t

I. INTRODUCTION

Microtubules (MTs) are long and extremely rigid, tubular polymers. They assemble from tubulin, a protein found in eukaryotic cells, which ''crystallizes'' to form a helical lattice (see Fig. 1). Microtubules form an important part of the cellular scaffold and provide a network of ''rails'' for active intracellular transport. They also play a crucial role during cell division, forming a dynamic structure that spatially separates duplicated chromosomes. Twelve years ago, Mitchison and Kirschner discovered that the polymerization of MTs from tubulin is a very unusual process: a MT can repeatedly, and apparently randomly, switch between persistent states of assembly and disassembly in a *constant* concentration of tubulin [1,2]. This behavior is observed *in vivo* as well as *in vitro* (see Fig. 2) and is referred to as *dynamic instability*.

This switching between growing and shrinking states at one concentration is unusual for a polymer. It is achieved by an increase in the chemical potential of the monomers after assembly. The energy required to do this is provided by hydrolysis of a guanosine triphosphate (GTP) nucleotide bound to assembling monomers. While thermodynamics thus can explain the coexistence of the growing and the shrinking states, it cannot explain the dynamics of the transitions between these states. An interesting possibility, suggested by Mitchison and Kirschner [1,2], is that transitions occur as a consequence of competition between assembly and GTP hydrolysis. A growing microtubule assembles by the addition of GTP tubulin, which is later converted to guanosine diphosphate (GDP) tubulin. In Mitchison and Kirschner's scenario, a growing microtubule has a stabilizing *cap* of GTP tubulin [2,3]. If hydrolysis overtakes the addition of new GTP tubulin, the cap is gone and the MT's end undergoes a change to the shrinking state, a so-called *catastrophe.* Though it is known that GTP hydrolysis precedes disassembly, it may not be the rate-limiting process in the change to a disassembly-favoring state, however. Conformational changes of tubulin or structural changes of the MT are other candidates; see [4–6] for reviews.

Despite the large amount of experimental and theoretical work devoted to the cap model, it is still the subject of controversy [4,5,11,12]. At the center of the debate are seemingly contradictory results about catastrophes, GTP contents, and the cap size coming from three types of experiments.

(i) When MTs are grown in pure GTP-tubulin solutions at various constant concentrations, the frequency of catastrophes is one every *few minutes* and decreases with increasing concentration [13,14]; see Fig. 4 below. This suggests that the stabilizing cap is longer, hence less apt to be lost, at

*Present and permanent address: Department of Optics and Fluid Dynamics, Risø National Laboratory, DK-4000 Roskilde, Denmark.

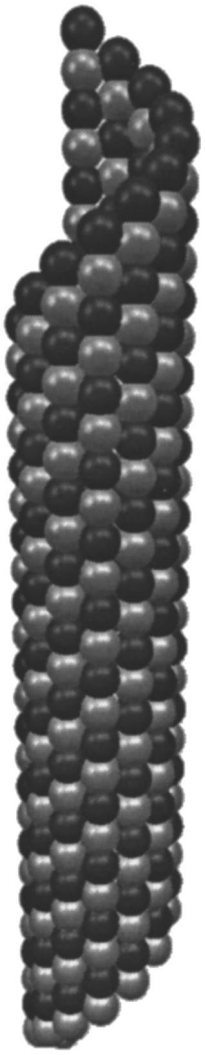

FIG. 1. Microtubule shown as five-start helical lattice of heterodimers, the so-called *A* lattice. Dimers are shown as vertical pairs of dark and light spheres, which represent monomers of α and β tubulin, and are arranged end to end in 13 so-called protofilaments [7]. Other lattice structures are possible [8,9].

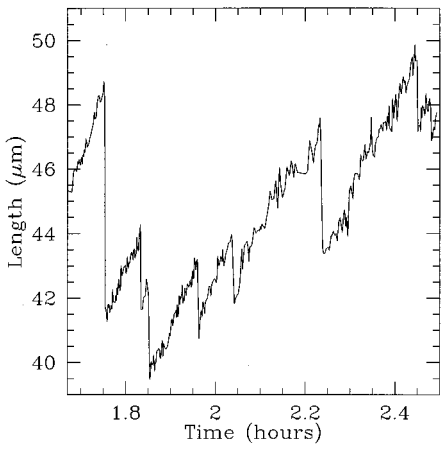

FIG. 2. Length as a function of time for a single microtubule. Data are from [10].

larger concentrations. But no cap model has been able to relate concentration with frequency of catastrophe in a manner quantitatively resembling the observed relationship.

(ii) In *dilution experiments* the concentration of tubulin is abruptly reduced to zero, resulting in catastrophes within *seconds*, independent of the initial concentration [15,16]; see Fig. 5 below. This suggests that the cap is short and independent of the concentration at which it is formed.

(iii) In experiments attempting to measure the GTP contents of microtubules grown in a manner to assure maximal GTP contents, no GTP can be found after the 15–20 s dead time of the experiment [17].

Successful models should also be able to explain a range of other observations: that the distribution of catastrophe times is nearly exponential [18], that a small cap assembled from a nonhydrolyzable GTP analog can stabilize a microtubule [19], that cutting a microtubule usually results in a catastrophe [20], and others.

In this article we show how these experiments are described naturally by the same simple stochastic cap model, thereby resolving these apparent contradictions. The wide temporal range of behavior of the first three experiments enumerated—from seconds to minutes—is explained in terms of tubulin assembly and transformation, processes that occur over time scales shorter than tenths of seconds. In formulating this model, we were inspired by the many previous attempts; see [4] for a review.

All mathematical derivations in the article itself are heuristic, with the emphasis on the modeling of mechanisms. But all heuristic results are backed by rigorous analysis given in the Appendixes.

Specifically, the article is organized as follows. Section II motivates our use of an effective theory and explains what it is, for the benefit of readers to whom the concept is unfamiliar. Section III introduces the theory, or model. Section IV presents a heuristic analysis of the model. It is an attempt to understand as much as possible from the assumed dynamics of the model, employing a minimum of calculations. Sections V–XI discuss specific types of experiments, essentially one type per section. In each section the experiments are briefly explained with the issues they address, we give the aspects of the model that are relevant for its comparison with the experiments in question, and discuss the comparison. We see a careful discussion of model and individual experiments in the light of each other as the only proper way to test the model and to isolate new experimental questions. Section XII contains the discussion. Section XIII lists suggested experiments. Section XIV contains our conclusions.

Appendix A collects our notation, which is introduced wherever needed throughout the article. Six additional appendixes contain the mathematical analysis of the model and its adaption to specific experimental situations. These appendixes provide the mathematical underpinning of the article, which no heuristic analysis can provide. The model presented in this article was described briefly, with an equally brief comparison with some experiments, in [21].

II. MICROTUBULE STRUCTURE AND MOTIVATION FOR AN ''EFFECTIVE'' THEORY

The general structure of a microtubule is shown in Fig. 1. It is a tube formed from dimers arranged in a helical pattern.

Each dimer consists of two closely related polypeptides, called α and β tubulin. In solution, these are bound very tightly together, and this tubulin dimer plays the role of the ''monomer'' of microtubule polymerization. We will use the two terms, dimer and monomer, interchangably. The dimers are arranged along the microtubule in a head-to-tail pattern, forming a ''protofilament.'' Microtubules in living cells usually have 13 protofilaments, but ones assembled *in vitro* may have a range of protofilament numbers.

The literature contains several rather detailed cap models; see [4,5] for reviews. *A priori*, the detailed accounting of these models for the fate of individual tubulin dimers may seem both necessary and advantageous. In practice, however, the experimental data available are insufficient to determine many free parameters. The available data do not provide direct information about the ''microscopic'' processes described by these models. The data were taken with light microscopes that are resolution limited to seeing changes of several hundred monomers. The microtubule itself is seen only as a change in optical density where it is located. The data also are not sufficiently precise to allow us to deduce the proper values of microscopic parameters from their ''macroscopic'' consequences.

We choose an alternative approach to modeling by aiming for an *effective* theory containing as few details as possible. By an effective theory we mean a theory that is not formulated in terms of fundamental variables and phenomena, but in terms of fewer variables on a coarser scale. Ideally, an effective theory and its parameters are then derivable from a fundamental, microscopic theory and *its* parameters.

Several data sets are available from experiments investigating different manifestations of the cap. None of the existing models have been able to explain more than selected aspects of the data. So the data can discriminate against models. On the other hand, it is clear from the data that a model should contain only a few free parameters if they are to be unambiguously determined by the fit. More parameters will result in ambiguities in their determination.

Thus we know that we should not be concerned with the details of the microtubule lattice. With its 13 protofilaments and its five-start helical structure for the lattice of tubulin dimers, we would have to introduce a multitude of parameters to describe the various cap configurations in such a microscopic description, as some models do [12,22]. We know, of course, that it is at this microscopic scale (and even smaller scales) that the relevant processes take place. The idea of a GTP cap model is that it is GTP molecules liganded to individual tubulin dimers that are hydrolyzed, thereby changing a given dimer from being part of the cap to no longer being that. But this does not oblige us to carry out our modeling at this microscopic length scale. That is why we aim for an effective theory.

The length scale that we here refer to as microscopic is the molecular scale of tubulin heterodimers, the monomers of the polymer that is a microtubule. It is 5–10 nm. The effective theory is formulated on a coarser length scale, unable to resolve the three-dimensional structure of a microtubule, which consequently is seen as a one-dimensional object.

III. AN EFFECTIVE THEORY

Since our goal is an effective theory, we only need the crudest description of what goes on at the microscopic level. To be specific, we are not concerned with the tubular shape of microtubules. Nor are we concerned with the dimer form of the tubulin, as the dimers effectively function as monomers in the polymerization process. We do, however, take into account a *consequence* of the heterodimer form of tubulin: it gives a definite overall *polarity* to the microtubule, with the consequence that its two ends differ, as illustrated in Fig. 1. In terms of structure, one end terminates in α tubulin, while the other terminates in β tubulin. In terms of dynamics, one end (conventionally called the plus end) polymerizes faster than the other (called the minus end). It is not yet clear whether the plus end is the α-terminating or β-terminating end. In the present section we formulate the model for one end without specifying which, since we describe both ends with the same model, with only some of the rate constants differing.

A. Microscopic description

Consider monomers that polymerize at one end with a rate constant k_g for addition, each contributing δx to the length of the polymer. Thus the polymer end will grow with average velocity

$$v_g = k_g \delta x. \tag{1}$$

The monomers in question are tubulin heterodimers, known to be 8 nm long, and we can assume a microtubule has 13 protofilaments. So we know that each monomer added to it contributes with $8\ \text{nm}/13 = 0.6\ \text{nm}$ to its length, i.e., we know that

$$\delta x = 0.6\ \text{nm}. \tag{2}$$

In a normal polymerization processes, the on rate k_g is usually accompanied by an off rate and the growth velocity v_g, which is observed in experiments, is the net effect of the competition between these two rates. However, in the case of microtubules it has been demonstrated experimentally that the off rate is zero [13]. Consequently, the value of k_g can be calculated from Eq. (1), since δx is known and v_g can be observed. This is important because k_g is more than just an alternative representation of the information contained in v_g. It parametrizes a random process, the addition of δx to the length of the microtubule. The *average* outcome of this process is described as continuous growth with constant velocity v_g. But superposed on this, there is the difference between the actual and the average outcome, an *un*biased random process that we will *not* ignore [23–25].

We think of the monomers as tubulin-t that will hydrolyze to tubulin-d since that is the general scenario of GTP cap models. But, strictly speaking, this does not matter for our effective theory. What matters is (i) that polymer ends grow by addition of monomers that are in *one* state, (ii) that these monomers, once added, can and will change to a *different* state, and (iii) that the first state keeps a growing microtubule-end growing, while (iv) the second state causes a ''catastrophe'' if it extends to the end of the microtubule. The difference between the two states needs not be the dif-

ference between GTP and GDP. It can, for example, be purely configurational [5]. In the remainder of this article we will continue to use the terms tubulin-t, tubulin-d, and hydrolysis as convenient terms for the two states and the passage from one to the other. But it should be remembered that we have not committed the effective theory to the literal meaning of these labels.

We assume that hydrolysis is a stochastic phenomenon, occurring with rate constant k_h where a tubulin-t monomer neighbors a tubulin-d monomer and rate constant k_h', where it does not; see Fig. 3. Thus a section of the polymer end that consists entirely of tubulin-t will hydrolyze from its borders with tubulin-d with average velocity

$$v_h = k_h \delta x, \tag{3}$$

where the value of v_h may depend (through k_h) on whether the border moves towards the plus or the minus end because of the inherent polarity of the microtubule. Below, we distinguish between those two cases with the notation $v_h^{(+)}$ and $v_h^{(-)}$. In general, this hydrolysis moving in a specific direction is referred to as *vectorial* hydrolysis.

In the interior of a section of polymer that consists of tubulin-t, new borders are formed with a rate

$$r = k_h' / \delta x \tag{4}$$

per unit length per unit time. This rate is the same at both microtubule ends, since it describes a process that is not oriented relatively to the microtubule's polarity. One might refer to it as *scalar* hydrolysis.

We do not know the values of the rate constants k_h and k_h'. They are model parameters that must be determined by fitting the model's results to experimental data. Since δx is known, v_h and r are an alternative pair of model parameters, entirely equivalent to k_h and k_h' as long as we keep in mind that k_h, like k_g, also parametrizes a random process, in this case the removal of δx from the length of a tubulin-t section of the microtubule. The velocity v_h describes the average outcome of this process, but we will also account for the fluctuations around this average in order to obtain catastrophes in growing microtubules.

Now consider a section of the polymer that consists entirely of tubulin-t and is located at the end of the polymer. It will be referred to as the cap. On the average, this cap grows with velocity

$$v = v_g - v_h, \tag{5}$$

but hydrolysis of its interior breaks it into a shorter cap and another section of tubulin-t at a rate rx, where x is the instantaneous length of the cap. The length of the resulting shorter cap is any fraction of x with equal probability since the process of interior hydrolysis that cuts the cap down in size occurs with equal probability anywhere along its length.

When the cap is cut into two pieces in this way, the ''piece'' of tubulin-t that is not the new, shorter cap is hydrolyzed from *both* its ends (see Fig. 3), as well as in its interior, while no new tubulin-t is added to it. So it disappears relatively fast, while new such patches of tubulin-t are left behind by the ever moving cap. We assume that if a catastrophe occurs and the end of the depolymerizing microtubule encounters such a leftover patch of tubulin-t, then this patch does *not* cause so-called rescue, i.e., it does not constitute a new cap that brings the microtubule end back in the growing state. On the contrary, we assume that the microtubule depolymerizes uninhibited by the patch. We imagine that the tubulin-d oligomers known to ''curl'' off depolymerizing microtubules gain sufficient energy by their change to this configuration that they, when bordering a patch of tubulin-t, are able to sever the lateral bonds between protofilaments made of tubulin-t. Thus the model presented here does not provide a mechanism for rescues, which presumably are due to an entirely separate phenomenon (consider the results of [26–28]).

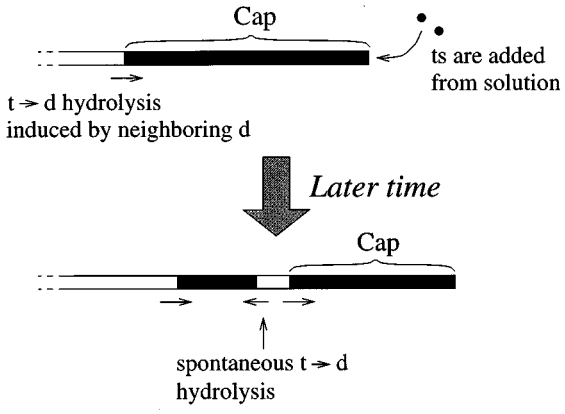

FIG. 3. Polymer consisting of tubulin-t and tubulin-d monomers of length δx, growing by the addition of tubulin-t monomers with rate k_g. Sections of tubulin-t hydrolyze to tubulin-d at a rate k_h from ends and rate k_h' from interior. Sections of tubulin-t inside polymer disappear by hydrolysis, while the end section, ''the cap,'' grows with velocity $v = v_g - v_h = (k_g - k_h)\delta x$ and is broken into a shorter cap plus another section of tubulin-t at rate $r = k_h'/\delta x$ per unit length per unit time. The cap grows with velocity v that is the difference between the velocity v_g with which the microtubule grows and the velocity v_h with which the ''hydrolysis front'' moves.

B. Getting rid of the microscopic description

Neither the rate r nor the velocities v, v_g, and v_h carry any information about the microscopic length scale δx, nor about the rates *per monomer* k_g, k_h, and k_h'. So as long as we use only the quantities r, v, v_g, and v_h in our description, we can ignore the existence of a microscopic scale. Mathematically formulated, we can take the limit $\delta x \to 0$ while keeping r, v, v_g, and v_h at fixed values; they are of order zero in δx.

We will, however, retain *one* consequence of the existence of the microscopic scale in our effective theory: While the length x of a cap *on the average* grows with velocity v between events of internal hydrolysis, *fluctuations* around this average are inevitable, but only of order one in δx, as Eq. (6) shows. So these fluctuations, which we retain in the description, are a signature of the microscopic phenomena underlying our effective description. One may view this description as a systematic approximation, resulting from an expansion in δx up to two leading orders.

As already indicated, the source of these fluctuations is the random nature of the events that the cap length x in a given time interval is extended by the amount δx by the addition of a tubulin-t dimer to the microtubule or reduced by δx by the hydrolysis of a dimer at the trailing edge of the cap. By a straightforward calculation one finds that the *variance* of this cap length distribution grows in time with a constant rate

$$2D=(k_g+k_h)\,\delta x^2=(v_g+v_h)\,\delta x, \tag{6}$$

i.e., the cap length evolves in time as the coordinate x of a particle diffusing in one dimension with diffusion constant D given in Eq. (6).

This completes the description of our model. Bringing it all together, a cap of length x grows steadily with velocity v, but also experiences two different stochastic processes: A diffusionlike time evolution, parametrized by the diffusion constant D, is superposed on the steady growth. With probability rx per unit time the length x of the cap will be reduced to any fraction of its length with equal probability. When we add to this description that a vanishing cap, the event that a cap's length x happens to decrease to zero, represents a catastrophe, then we have fully described our model.

IV. HEURISTIC ANALYSIS OF THE MODEL

This section attempts to develop some understanding of how our model works through a heuristic analysis of it. A rigorous analysis of the model is given in this article's appendixes and the results of this analysis are discussed in the following sections, where we see that the heuristic estimates derived in this section are quite accurate.

A. Dynamically coupled hydrolysis

We notice that according to our model, the GTP in a growing microtubule is located not only in the cap, but also in other ''patches'' of tubulin-t surrounded by tubulin-d; see Fig. 3. The GTP in these patches was recently a part of the cap, but was separated from it by its internal scalar hydrolysis. Once separated from the cap, such patches of tubulin-t suffer vectorial hydrolysis from both ends and internal scalar hydrolysis as well. Internal hydrolysis breaks patches into more patches, all of which hydrolyze from both ends and internally as well. The result is a total rate of GTP hydrolysis per microtubule end, which can be substantially larger than the rate of GTP hydrolysis taking place in the cap alone.

We assume the hydrolysis rates $v_h^{(\pm)}$ and r are independent of the growth rates $v_g^{(\pm)}$ of a microtubule's plus and minus ends, i.e., we assume *uncoupled hydrolysis.* So at large growth rates $v_g^{(\pm)}\gg v_h^{(\pm)}$, microtubule ends would grow caps at rates $v_g^{(\pm)}-v_h^{(\pm)}$ were there no internal hydrolysis. With a nonvanishing rate of internal hydrolysis, however, a GTP cap of length x suffers internal hydrolysis at rate rx, as does any other patch of tubulin-t of length x. With every event of internal hydrolysis two new ''fronts'' of ''vectorial'' hydrolysis are opened up, thereby adding

$$w_h\equiv v_h^{(+)}+v_h^{(-)} \tag{7}$$

to the total rate of GTP hydrolysis at the microtubule end in question; see Fig. 3. So a plus or minus end equipped with a tubulin-t cap and $n^{(\pm)}$ additional patches of tubulin-t will hydrolyze GTP at the rate

$$v_{h,\mathrm{eff}}^{(\pm)}\equiv v_h^{(\pm)}+n^{(\pm)}w_h\,. \tag{8}$$

For a microtubule end elongating at a given rate $v_g^{(\pm)}$, the number $n^{(\pm)}$ of tubulin-t patches trailing the cap is a fluctuating integer. New patches are created by the stochastic process of internal hydrolysis. Because they are created with stochastic lengths, they also disappear at stochastic times, even as they shrink with constant velocity $v_h^{(+)}+v_h^{(-)}$. However, we know the *average* value of $n^{(\pm)}$ in a state of steady growth. Since tubulin-t is added to a microtubule end at the rate $v_g^{(\pm)}$, it must, on the average, also hydrolyze at that rate in the steady state, so

$$\langle v_{h,\mathrm{eff}}^{(\pm)}\rangle=v_g^{(\pm)}, \tag{9}$$

from which it follows that

$$\langle n^{(\pm)}\rangle=\frac{v_g^{(\pm)}-v_h^{(\pm)}}{w_h}. \tag{10}$$

Thus we see that, although we have assumed that hydrolysis is a simple stochastic process, characterized by rates that are uncoupled from the rates of microtubule growth, we nevertheless end up with a total rate of hydrolysis at each microtubule end that is *dynamically coupled* to its growth rate. All that is required to have this phenomenon is *two kinds* of uncoupled hydrolysis: the internal scalar hydrolysis occurring at a rate proportional to the amount of GTP present and the vectorial hydrolysis occurring at each interface created by the scalar hydrolysis. As we shall see, this also results in a short cap and a finite catastrophe rate at all growth rates.

B. Cap size

We expect qualitatively different dynamics for different values of the three parameters v, D, and r. Intuitively, we might expect there to be three regimes of behavior. One is a *large-positive-velocity* regime, in which the cap grows quickly in length and only the cutting prevents the cap from becoming large. In this regime, the ''diffusion'' of the cap length is less important for its length than its average growth and its cutting. Another regime is the *large-negative-velocity* regime, in which the cap shrinks on average and only the fluctuations allow the cap to exist at all, but it remains so short and short lived that cutting is unimportant. Finally, we expect a *small-velocity* regime, in which diffusion and cutting are most important because the average growth is small.

It is interesting to understand the behavior of the model in all three of these regimes, as they all turn out to be relevant for the interpretation of experiments. It also turns out that we can calculate a great deal using only dimensional analysis, since each of the three regimes is characterized by the dominance of two of the three parameters. As a first example, we calculate the cap size in the large-velocity regime.

Basically, any cap grows with average velocity v. But its length x is kept within bounds by its abrupt reduction by interior hydrolysis to any fraction of x with rate rx. With

Δt denoting the average time between such reductions of the cap length, we have the estimate

$$r\langle x\rangle\Delta t\approx 1, \tag{11}$$

where $\langle x\rangle$ is the average cap length.

Between reductions, caps grow with velocity v, hence with the length $v\Delta t$, on the average. This is also the length removed when a cap is reduced from its largest length to, on the average, half that length, from which it grows again. So its largest length we estimate by $2v\Delta t$, its shortest to half that, and consequently its average length we estimate as

$$\langle x\rangle\approx 3/2v\Delta t. \tag{12}$$

Eliminating Δt, we find for the average cap length

$$\langle x\rangle\approx\sqrt{\frac{3v}{2r}}. \tag{13}$$

This equation shows that the cap length grows only slowly with the microtubule growth rate v_g, which enters through Eq. (5).

The averages we here have listed freely with the phrase ''on the average'' are not rigorous averages, but estimates. They are better than order-of-magnitude estimates, but they are not exact in general.

Note that the estimate given in Eq. (13) is the only combination of v and r that we can create that has units of length, so we could have guessed this form of the result from the beginning, apart from its numerical prefactor, since we have excluded D from the argument as being irrelevant at large velocities v. We can use this observation to calculate the cap size in the other two regimes: only D and r will enter in the small-velocity regime and only v and D will enter in the large-negative-velocity regime, for the reasons given above. Dimensional analysis thus tells us that the average cap size is given by

$$\langle x\rangle\sim\begin{cases}\left(\dfrac{v}{r}\right)^{1/2} & \text{in the large-positive-velocity regime}\\ \left(\dfrac{D}{r}\right)^{1/3} & \text{in the small-velocity regime}\\ \dfrac{D}{|v|} & \text{in the large-negative-velocity regime.}\end{cases} \tag{14}$$

The cap size grows as v increases, so the cap is smallest in the large-negative-velocity regime and largest in the large-positive-velocity regime.

If we take the ratio of two of these length scales, we have a dimensionless quantity. We define this quantity as

$$\gamma=\frac{v}{2(D^2r)^{1/3}}, \tag{15}$$

where the factor of 2 is for convenience later. γ is a measure of the importance of v relative to the other constants and allows us to make precise our definition of the regimes. In particular,

$$(\text{large positive velocity})\leftrightarrow\gamma\gg 1, \tag{16}$$

$$(\text{small velocity})\leftrightarrow -1<\gamma<1, \tag{17}$$

$$(\text{large negative velocity})\leftrightarrow\gamma\ll -1. \tag{18}$$

C. Catastrophe rate

The cap size, however important conceptually, is not directly observable for GTP caps. (Stabilized caps are discussed below.) The catastrophe rate is, so it is useful to have a simple way of estimating the catastrophe rate. The important step is to realize that it is the fluctuations parametrized by D that cause catastrophes when v is positive, since the cap grows on the average, and there is no chance that the cap will be cut to exactly zero length. But because caps effectively are bounded in length because of internal hydrolysis and because the growth of caps really is a biased random walk, any cap will vanish sooner or later. So we have a nonzero catastrophe rate in this model.

We assume the cap starts with a size of order $\langle x\rangle$. For $v>0$ the catastrophe rate then is the average time required for the cap to fluctuate in size by this amount $\langle x\rangle$, which is on the order of $D/\langle x^2\rangle\sim D/\langle x\rangle^2$.

In the case $v<0$, the cap shrinks on the average and this alone, without fluctuations, will cause a catastrophe in a time $|v|/\langle x\rangle$. Therefore,

$$f_{\text{cat}}\sim\begin{cases}\dfrac{D}{\langle x\rangle^2}=\dfrac{Dr}{v} & \text{when } \gamma\gg 1\\ \dfrac{D}{\langle x\rangle^2}=(D^2r)^{1/3} & \text{when } -1<\gamma<1\\ \dfrac{|v|}{\langle x\rangle}=\dfrac{v^2}{D} & \text{when } \gamma\ll -1.\end{cases} \tag{19}$$

The catastrophe rate is smallest when $\gamma\gg 1$ and largest when $\gamma\ll -1$.

D. Delay time for dilution-induced catastrophes

In dilution experiments caps are grown at velocity v and then have their growth retarded or arrested by dilution of the surrounding tubulin solution to a low or vanishing concentration, which we characterize by its resulting (possibly negative) growth velocity v' for the cap. We estimate the average delay between dilution and ensuing catastrophe. v' corresponds to γ' and the value of γ' determines which parameters dominate. For sufficiently strong dilution, $\gamma'<-1$ and the cap is consequently cut until its length is short enough that its negative growth velocity causes it to disappear before the next cutting event, i.e., it is cut to a length x given by

$$\frac{1}{rx}\sim\frac{x}{|v'|}\Rightarrow x\sim\sqrt{\frac{v'}{r}}. \tag{20}$$

Therefore the delay time for a dilution induced catastrophe is approximately $1/\sqrt{|v'|r}$.

E. Amount of GTP in a microtubule

While we do not specify the chemical or structural nature of the cap in our model, one possibility is that it is defined by the tubulin-t subunits. If so, we can use the model to estimate the amount of GTP present in a microtubule. In experiments designed to measure this quantity, microtubules are grown from tubulin-t in which the GTP is radioactively labeled. The GTP content of the microtubules grown this way is measured by filtering them from the surrounding tubulin solution, washing the filters, and then measuring the level of radioactivity. Thus some time passes, and consequently GTP hydrolysis, between the time when the microtubules have their growth arrested and the time when the GTP content is measured. We estimate the amount of GTP left in a microtubule as a function of time t after dilution.

The tubulin-t in a microtubule exists as a cap on each end, shrinking from their trailing edges with velocities $v_h^{(+)}$ and $v_h^{(-)}$, respectively, plus a number of GTP ''patches,'' each of which shrinks from its edges with velocity $v_h^{(+)}$ on one side and $v_h^{(-)}$ on the other. Furthermore, each cap and patch is broken into smaller caps and patches at rate r per unit length. It is possible and convenient to treat the two caps as *one* patch with the caps' summed length, because this ''effective'' patch shrinks with the same velocity w_h as do the other patches.

Let $n(t)$ denote the total number of patches at time t, including that made from the caps, and let l_{GTP} denote the total length of tubulin-t left at time t. These numbers differ for different microtubules, but we let $n(t)$ and $l_{\mathrm{GTP}}(t)$ denote the *average* value at time t, the average being taken over a large number of microtubules, i.e., an ensemble average. Then $n(t)$ is a real number, varying continuously with t. The total amount of tubulin decreases at the rate

$$\frac{dl_{\mathrm{GTP}}}{dt} = -w_h n(t) \tag{21}$$

and the number of patches changes as

$$\frac{dn(t)}{dt} = rl_{\mathrm{GTP}}(t) - (\text{loss term}). \tag{22}$$

The loss term describes the rate at which patches disappear by shrinking to zero length. It depends on the distribution $n(xt)$ of patch lengths x—it is $w_h n(0,t)$, to be specific and hence cannot be expressed in terms of the two variables n and l_{GTP}. So the simple equations we just gave do not close.

Dimensional analysis is also insufficient to save the day, though the time scale obviously is set by

$$t_h \equiv (rw_h)^{-1/2} \tag{23}$$

because the GTP will hydrolyze significantly faster if it initially is distributed over many relatively short patches rather than a few relatively large ones.

The patch length distribution needed for initial condition here is determined in Appendix F for a microtubule growing with constant velocity and having done so long enough for a steady-state to have been achieved. It is found to be rather complicated. $n(0)$ we know, of course, for this steady-state growth from Eq. (10). But we do not even know the total amount of GTP present initially, hence we cannot even give an upper bound on the time it takes for it to hydrolyze, say, by assuming it is all located in one big cap. So we finish this section on heuristic analysis with a clear-cut case of its failure.

V. CATASTROPHE RATE

A. Connecting theory and experiment

The frequency at which microtubules change from their growing to their shrinking state, the catastrophe rate, is best measured experimentally by observing the dynamics of individual microtubules [29,30,14,13]. We focus here on the latest results [13]. The catastrophe rate is found as the ratio between the total number of catastrophes observed in an experiment and the total time spent in the growing state by the microtubules observed. In this experiment microtubules are grown from seeds and a shrinking microtubule always vanishes entirely, whereupon a new microtubule grows from the seed.

This is a crucial observation because it makes it possible to establish the necessary connection between theory and experiment. This is a nontrivial matter: Because the model is formulated as a partial differential equation, initial data and boundary conditions are required to determine the particular solution to this equation, which describes a given experimental situation. We meet this requirement in the following way.

(i) As just observed, we may assume that each cap is initially created with zero length, because it is created on a microtubule starting its seeded growth from zero length. This means that the ensemble of caps found on microtubules grown this way is described by Eq. (C18).

(ii) The microtubules that are observed in the experiment have caps that are as old as the microtubules themselves, since the experiment was carried out under conditions where rescues do not occur. So the individual cap has aggregated and lost again by hydrolysis as much tubulin-t as there is tubulin in its microtubule. This means that the cap is *old* by its own standards, by which we mean that the probability distribution for its length has the asymptotic form given in Eq. (D1), with the result that the catastrophe rate is given by Eqs. (D3) and (D5),

$$f_{\mathrm{cat}} = Dr/v = \frac{r\,\delta x(v_g + v_h)}{2(v_g - v_h)}. \tag{24}$$

B. Characteristic features of theoretical result

The catastrophe rate given in Eq. (24) has a nonzero limit $r\,\delta x/2$ for $v_g/v_h \to \infty$ and becomes large for $v_g \to v_h$. This is in agreement with experimental results, which show that f_{cat} seems to be constant for higher tubulin concentrations, while f_{cat} increases rapidly if v_g is decreased to small values; see [13], Fig. 7, which is reproduced in Fig. 4.

Equation (24) gives an infinite value for f_{cat} for $v_g = v_h$, corresponding to $v = 0$. This, however, is an artifact originating in Eq. (24) being an approximation valid only for γ large. For $v \approx 0$, γ is not large, hence the approximation is not valid. In dynamical terms, the approximation assumes the cap sustained by its growth with v alone, and this is not true for small values of v, as explained heuristically above.

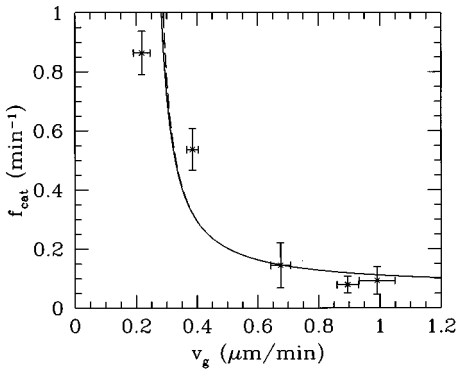

FIG. 4. Catastrophe rate $f_{\rm cat}$ versus growth rate v_g. Dots with error bars represent experimental results [13]. The horizontal error bars represent the standard error in the mean (SEM) $v_{\rm g}$ for the sample, the vertical error bars the SEM for the catastrophe rate. The full curve represents the theoretical expression from Eq. (D8) with $t_{\rm cutoff}=0.1$ μm. A plot of the approximate theoretical expression in Eq. (D3) cannot be distinguished from the full curve, showing how well Eq. (D8) is approximated by it. The dashed curve represents the theoretical expression from Eq. (24) approximating Eq. (D3). Note that this graph is a hyperbola. All three theoretical expressions were fitted to the experimental results, using $\delta x=0.60$ nm, and resulted in $v_h^{(+)}=0.25\pm0.05$ μm/min and $r=222\pm84$ $\mu{\rm m}^{-1}{\rm min}^{-1}$ for the optimal fit of Eq. (24). The other two fits gave the same result up to insignificant differences.

Diffusion also contributes to a finite cap length and is the dominant effect for small values of v. How precisely this happens is described by the full expression given in Appendix D. For the present, we have understood that Eq. (24) is valid only when γ is not small, i.e., when v_g is not too close to v_h. The value for v_h is determined in the following subsection.

C. Comparing the theory to experimental results for the catastrophe rate

We have fitted the expression for the catastrophe rate in Eq. (24) to the experimental results for the catastrophe rate for plus ends $f_{\rm cat}^{(+)}(v_g^{(+)})$, given in [13], Fig. 7, and shown in Fig. 4, by treating $v_h^{(+)}$ and r as fitting parameters. The resulting fit is seen in Fig. 4, and we see that there is satisfactory agreement between theory and experiment, when we remember that the experimental error bars do not denote random Gaussian errors, but only are the best we could come up with for error bars: The data that were averaged to get the data points shown contained some scatter and we treated this scatter as if it were due to truly random Gaussian errors. Also shown in Fig. 4 are fits based on the full expression in Eq. (C18).

With the superscript + on $v_h^{(+)}$ we have indicated, as above, that it is possible that the value for this hydrolysis rate may depend on whether it describes a hydrolysis front propagating towards a plus end, as here, or towards a minus end, because of the polarity of microtubules. On the other hand, we assume that the *interior* part of caps on plus and minus ends are identical. Thus the parameter r should be the same for plus and minus ends. As δx denotes the contribution from the length of a tubulin dimer to the length of the microtubule, it obviously is also the same for both ends.

As a matter of fact, the two velocities $v_h^{(+)}$ and $v_h^{(-)}$ *must* differ for the model to reproduce experimental results correctly: For a given tubulin-t concentration, the growth rate $v_g^{(-)}$ for the minus end is slower than the growth rate $v_g^{(+)}$ for the plus end by approximately a factor 2 (see [14], Fig. 4). If the hydrolysis rate v_h were the same at both ends, our model would predict a higher catastrophe rate for the minus end than for the plus end because of the minus end's slower growth rate. But the minus end seems to have the same or smaller catastrophe rate as the plus end at a given tubulin-t concentration (see [14], Fig. 7). So our model leads us to conclude that $v_h^{(-)}$ is approximately twice as small as $v_h^{(+)}$ This conclusion should be taken with the precaution that the error bars on the experimental results in [14], Fig. 7 are large. But the arguments just presented illustrate well a general point.

We expect $v_h^{(+)}$, $v_h^{(-)}$, r, and, obviously, δx to be independent of the tubulin concentration, so the model must account for the experimentally observed difference between catastrophe rates at plus and minus ends solely through the experimentally observed difference in growth rates $v_g^{(+)}$ and $v_g^{(-)}$ because only through these rates does the model depend on the tubulin concentration. This demand on the model provides an acid test of it, so it would be interesting to have data to test it against.

Notice that even as we distinguish between plus- and minus-end values for v_g and v_h, the asymptotic values for the catastrophe rates $f_{\rm cat}^{(+)}$ and $f_{\rm cat}^{(-)}$ for $v_g^{(\pm)}\gg v_h^{(\pm)}$ are *the same* for plus and minus ends since they are given entirely in terms of δx and r in Eq. (19). This very distinct prediction of our model is consistent with experimental results; see [14], Fig. 7 and [31], Fig. 5. These results are not that precise, however, and the validity of this prediction is another experimental acid test of the model. To the extent the model survives the test, such an experiment is a very direct way to measure the parameter r.

VI. DILUTION EXPERIMENTS

In dilution experiments, microtubules are first grown in a high concentration of tubulin, giving a high assembly rate v_g, and then submitted to rapid and massive dilution to induce catastrophes and disassembly [15,16]. Dilution experiments were motivated by the *extended cap* model resulting from so-called *uncoupled vectorial hydrolysis*, which essentially is the model one obtains by setting $r=0$ in the model presented here. In that model hydrolysis only occurs from the trailing edge of the cap, at the rate v_h, which is not coupled to the growth rate v_g. Consequently, long caps, and correspondingly long delay times upon dilution, were expected for high growth rates. No such connection between predilution growth rates and ensuing catastrophe rates has been found. Quite to the contrary, the catastrophe rate upon dilution is essentially independent of the growth rate [16]. This observation was an important guide in formulating our model. In the present section we demonstrate that the model explains what is seen in dilution experiments. We concentrate on the latest work with the most detailed data [16].

In Appendix E the model is solved with boundary condi-

TABLE I. Parameter values of the model found by fitting to the experimental data as follows: first line, fit to experimental catastrophe rate for the plus end [13] with δx kept fixed at its experimental value 1 μm/1680 = 0.60 nm; second line, fit to the experimental waiting-time distribution for dilution induced catastrophes at the plus end [16] with δx kept fixed at its experimental value; third line, same as for the minus end; fourth line, combined fit to the experimental catastrophe rate for plus ends and the experimental waiting-time distributions for both ends, with δx fixed at its experimental value; fifth line, same, except that δx is also treated as a fitting parameter.

Figure	δx (nm)	r (μm^{-1} min^{-1})	$v_h^{(+)}$ (μm/min)	$v_h^{(-)}$ (μm/min)	$rv_h^{(+)}$ (min^{-2})	$rv_h^{(-)}$ (min^{-2})	t_h (s)
4	0.60	222±84	0.25±0.05		⇒56±24		
5	0.60				122±12		
5	0.60					101±10	
6	0.60	320±20	0.24±0.01	0.25±0.01	⇒76±6	⇒79±6	⇒4.8±0.2
	0.24±.03	514±76	0.26±0.02	0.21±0.01	⇒133±22	⇒108±17	⇒3.9±0.2

tions appropriate for dilution experiments. It is argued that a description even simpler than our full model suffices when microtubules are grown so fast before dilution that catastrophes can be ignored and when dilution is to a concentration so small that after dilution caps disappear mainly by cutting with rate r and shrinking with velocity $v' \approx -v_h$. In that case, fluctuations parametrized by D can be ignored, i.e., $D=0$ can be assumed. This simplifies our master equation (C1), resulting in simple solutions that are simple to find.

The relevant results are that the average delay time for dilution-induced catastrophes is

$$t_{\mathrm{cat}} = \left[\frac{-2rv'}{\pi} \left(1 - \frac{v'}{v} \right) \right]^{-1/2} \simeq \left(\frac{\pi}{-2rv'} \right)^{1/2}, \qquad (25)$$

where v and v' are the cap-growth velocities before and after dilution, respectively. The last approximate expression

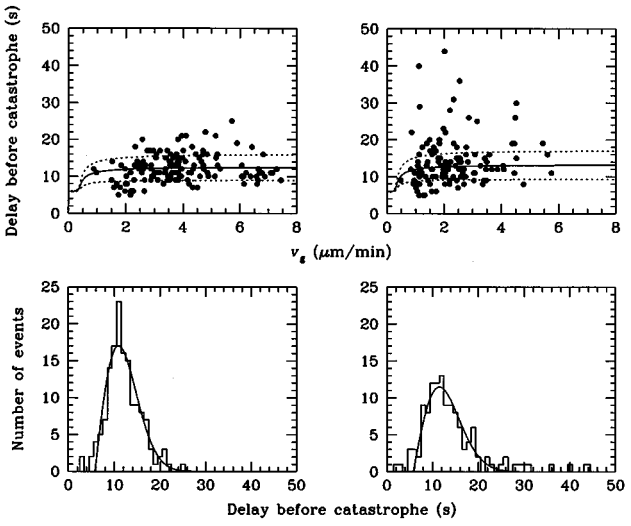

FIG. 5. Delays before the catastrophe following dilution. Data are taken from Ref. [16]. Left, plus end; right, minus end; top, delay as a function of initial growth velocity. Each point represents a single measurement on a MT. Curves are theoretical mean (solid) and standard deviation (dashed) of the delay, from Eqs. (25) and (26). Bottom, histograms showing the experimental distribution of delays before catastrophe. The curves are fits of the theoretical distribution given in Eq. (26) and result in parameter values given in Table I. Dilution was initiated at $t=0$ and required some time (6.1 s when used as a free parameter in our fit) for completion.

is typically a good approximation because the growth rate prior to dilution v_g typically is large compared to v_h and hence so is $v = v_g - v_h$, while dilution results in a small or vanishing concentration, resulting in $|v'| \sim v_h$ and therefore $v \gg |v'|$. Equation (25) therefore predicts a waiting-time distribution that is essentially independent of the growth rate prior to dilution. To the extent a dependence is predicted, the waiting time increases only slightly with the predilution growth rate v, except at small rates $v \sim v_h$; see Fig. 5. The delay time itself is a random number distributed as

$$p_{\mathrm{cat}}(t) = \frac{\pi t}{2t_{\mathrm{cat}}^{\,2}} \exp\left(-\frac{\pi t^2}{4t_{\mathrm{cat}}^{\,2}} \right). \qquad (26)$$

These theoretical results are in full agreement with the experimental results presented in [16], Figs. 3 and 4 and reproduced here in Fig. 5. In generating the theoretical curves, we assume that dilution stops all additional growth. This is probably correct under the conditions of the experiment [32].

It would be interesting if the nonlinear dependence we predict with Eq. (25),

$$t_{\mathrm{cat}}(v_g) = \sqrt{\frac{\pi (v_g - v_h)}{2r(v_h - v_g')(v_g - v_g')}}, \qquad (27)$$

could be fitted to the experimental data with statistically significant values for r, v_h, and v_g'. From the appearance of the data, we judge this not to be the case. The combination of parameters rv', on the other hand, is well determined from the essentially constant value of t_{cat} for large values of v_g.

Because the experimental delay-time distributions in the upper row in Fig. 5 to a good approximation is independent of the predilution growth rate $v_g^{(\pm)}$, the merger of these data, shown in the lower part of Fig. 5, should also be described by the distribution of delay times given in our Eq. (26), as long as one takes into account that the origin on the time axis in Fig. 5 denotes the starting point for a dilution that takes several seconds to reach completion. We have fitted our expression in Eq. (26) to the data in Fig. 5, leaving the ''true'' dilution time as a free parameter to be fitted, but using the same dilution time for the data for plus and minus ends, since the experiments were done with the same apparatus. Our fits are shown in Fig. 5.

From the values for t_{cat} giving the optimal fits shown in Figs. 5(c) and 5(d) and by assuming $v' = -v_h$, we find

$rv_h^{(+)} = 122 \pm 12\ \mathrm{min}^{-2}$ and $rv_h^{(-)} = 101 \pm 10\ \mathrm{min}^{-2}$. But since the two experiments giving the data in Figs. 4 and 5 were done under somewhat different conditions (e.g., there were differences in the buffers that may affect the dynamics [33–35]), we cannot expect the values for r and $v_h^{(+)}$ that we determined in Sec. V to agree with the value found here for the product $rv_h^{(+)}$, and indeed they differ; see Table I.

It would obviously be of great value to have experimental results taken under the same conditions for both the catastrophe rate, as in Fig. 4, for the delay time upon dilution, as in Fig. 5, and preferably for both microtubule ends. If the tubulin concentration after dilution can be known with reasonable certainty in the dilution experiment, such data would greatly overdetermine the three parameters r, $v_h^{(+)}$, and $v_h^{(-)}$ of the model and consequently provide another stringent test of it.

In conclusion, we have seen that the rather detailed data obtained by video microscopy in dilution-induced disassembly experiments all can be understood within our model. In particular, we have demonstrated that the delay in the onset of disassembly is a stochastic quantity whose average and distribution is quite well determined when the experimental data are interpreted in terms of our model. So the ''puzzling large variability'' [5] in the individual delay times that have been measured has a natural explanation within our model and the delay time *can* be determined from the data; it is not just a fixed number, but a random number with a known distribution. We have also explained quantitatively how the delay in the onset of disassembly depends on predilution concentrations and found that it does not, to a very good approximation. We have seen that the mechanism of cap hydrolysis that is responsible for the delays' near independence of predilution concentration is the very same mechanism that keeps the cap short irrespective of the concentration it is grown at, namely, interior hydrolysis at a constant rate r per unit length of cap.

In view of the good agreement between theory and experiment in Fig. 5 it would be interesting to have more experimental data for better statistics, especially for a range of small predilution growth rates where the model predicts a nontrivial dependence in the waiting-time distribution and a more complicated distribution. The quickest possible dilution is desirable in such experiments to obtain a sharper definition of the point in time where dilution effectively takes place. Alternatively, a controlled and calibrated dilution will do as well, since we can calculate the theory's prediction for any known tubulin concentration as a function of time, using the full theory presented in the Appendixes.

VII. COMBINED ANALYSIS OF THE CATASTROPHE RATE AND DILUTION EXPERIMENT

In this section we ignore the fact that the conditions differ between the two experiments giving the data shown in Figs. 4 and 5 and do a combined fit of the parameters three parameters to both data sets. Figure 6 shows the result as full curves, with dashed curves indicating the fits found in previous sections by separate fits. We see that the difference is not radical, but nevertheless significant. This reemphasizes the desirability of having both types of experimental data taken under the same conditions. The difference is also reflected in the different result obtained for the three parameters r, $v_h^{(+)}$, and $v_h^{(-)}$; see Table I.

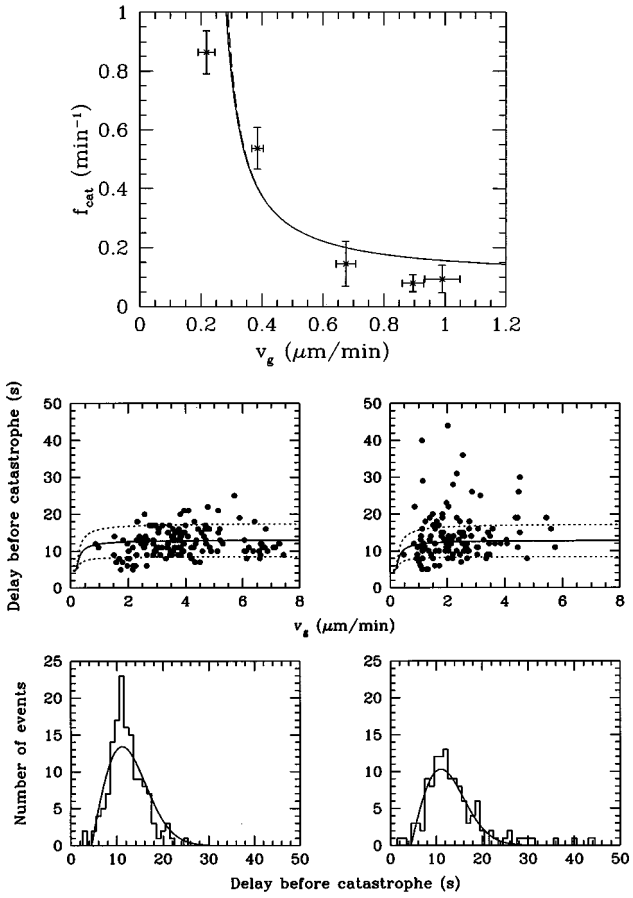

FIG. 6. Simultaneous fit of the theory to data for the catastrophe rate and data for the waiting-time distribution for dilution-induced catastrophes, using one pair of parameters r and $v_h^{(+)}$. Their fitted values are given in Table I. Top frame, catastrophe rate for the plus end of the microtubule; experimental data from [13]. Bottom four frames, waiting-time distributions as in Fig. 5 [36].

Since the combined fit overdetermines the three parameters, we can make a strong test of the robustness of the theory's description of the experimental data: We can use the excess of information available to fit also the value of δx to the data to see if its known value 0.60 nm, can be extracted from the data. We emphasize that this is a strong test because the data were taken with light microscopes with a resolution of several hundred nanometers, while the value for δx is known to be only a fraction of a nanometer. But with sufficiently many and sufficiently precise data points, a *correct* theory must, of course, be able to ''predict'' its own underlying microscopic length scale from a fit to the data. Conversely, if the data are insufficient or the theory's description of the data is shaky, the result of turning loose a parameter such as δx may result in a better fit, for sure, but with a physically absurd result for δx.

Fitting this way, we find $\delta x = 0.24$ nm. All in all, we find this value for δx close enough to the true one to give good support for the model. It is also yet another argument for the desirability of having data all taken under identical conditions.

VIII. GTP HYDROLYSIS RATE EXPERIMENTS

A. Issues

The suggestion that there is a GTP cap at the end of a polymerizing microtubule originated in a study of the kinetics of GTP hydrolysis [3]. The suggestion that the loss of this cap is the cause of catastrophe [2] inspired additional studies of the kinetics of GTP hydrolysis in assembling microtubules [37–43,17]. The conflicting results of these studies inspired several different models for the GTP cap [44–47,41,43,48,22,49]. The first study's suggestion of *uncoupled stochastic hydrolysis* [3] was replaced by *uncoupled vectorial hydrolysis*, *coupled* (or *forced*) *hydrolysis with stochastic dissociation*, and the related *lateral cap*; see [5,4] for reviews. In the present section we derive what our model can tell us about the kinetics of GTP hydrolysis. Thus we take a model has already proven its value by explaining microtubule behavior—experiments in which GTP hydrolysis plays a central role, but manifests itself only indirectly through the catastrophe rate and the waiting-time distribution—and we compare this model's predictions for hydrolysis experiments with the experimental results, *without fitting any parameters* or making any other adjustments. We emphasize that our model does not actually specify the biochemical nature of the cap, but if we suppose it to consist of GTP tubulin, then our model predicts the rate of GTP hydrolysis. We demonstrate that the model predicts GTP hydrolysis to follow assembly closely, in agreement with the most recent experimental results [38,39,42], because the initial lag period for hydrolysis lasts only a few seconds. We also demonstrate that the model explains the most recent and careful experiment attempting to measure the GTP contents of microtubules [17].

A key experimental issue concerns whether GTP hydrolysis follows microtubule growth closely or lags behind it at high growth rates. If the rate of GTP hydrolysis in a microtubule is independent of its rate of growth, hydrolysis may lag far behind the addition of GTP in a rapidly growing microtubule, especially if hydrolysis occurs only at the trailing edge of a cap, the case of *uncoupled vectorial hydrolysis*. But also *uncoupled stochastic hydrolysis* should result in microtubules containing a high proportion of GTP initially in the case of rapid growth. Consequently, it should be possible to detect the presence of GTP in rapidly growing microtubules as a lag in the amount of GTP hydrolyzed relatively to the amount of polymer assembled.

Whether or not hydrolysis lags behind assembly is a controversial issue; see [5,4] for reviews. The two most recent studies use radioactively double labeled GTP and rapid filtration techniques, but come to opposite conclusions. In [43] a significant lag in the release of phosphorus is reported. The technique used in this experiment has a dead time of only 2. This speed was acquired at a cost: filters were not washed and the raw data had to be corrected by large factors for contamination of the filtered microtubules with unpolymerized tubulin-t. In [17] it is reported that no accumulation of microtubule-bound GTP could be detected with a similar technique in which filters were washed and the dead time was 15–20. In the following subsections we first derive our model's predictions for hydrolysis rates and GTP contents and then discuss the experimental results in the light of our predictions.

B. Relevant quantities

Two aspects of the mode of hydrolysis described by our model are of particular interest for a discussion of experiments on the kinetics of GTP hydrolysis.

(i) How fast is the steady state pattern of GTP hydrolysis acquired upon the initiation of growth? Is an initial lag in hydrolysis detectable?

(ii) How fast does the GTP at the end of a growing microtubule disappear by hydrolysis, if growth is arrested? Will a method looking for this GTP in microtubules be able to detect it, given the dead time of the method between the arrest of growth and the measurement of GTP?

In order to answer these questions we must describe quantitatively how the patches of GTP fare in our model.

C. Case of microtubules growing at a constant rate

In this subsection we consider the GTP content of microtubules growing with constant velocity, i.e., in a constant concentration of tubulin. In actual experiments the tubulin concentration is depleted by the growth of microtubules [17,43,40]. This does not affect our evaluation of the initial lag time in hydrolysis given here if the characteristic time for depletion is much longer than the lag time. It does make a difference if the two characteristic times are comparable, as is the case in [17,43,40], because the GTP content is reduced by the reduction in the growth rate cased by depletion. The effect can be described along the lines used in this subsection; this is done in appendix G. The expressions given there are unwieldy, we warn the reader. One purpose of that Appendix is to show this, so the reader will settle for less in the present subsection. Another purpose of Appendix G is to give those unwieldy expressions for the record, since they do describe what happens in the relevant experiments. Here we merely observe that the initial lag time for hydrolysis derived here for microtubules growing at constant rate is an *upper bound* on the lag time for microtubules growing at the same rate initially, but then at decreasing rate. This bound comes about because the lagging hydrolysis has only to catch up to a lower rate of GTP incorporation in the microtubule than the initial one.

Consider now a microtubule end that grows with constant velocity v_g. At a distance l from the end of the microtubule, hydrolysis has been going on for a time l/v_g. Consequently, with the notation and results of Appendix F, at distance l from the end of the microtubule we expect to find a total length $\chi(t=l/v_g)$ of tubulin-t per unit length of microtubule, distributed over a total of $n(t=l/v_g)$ patches per unit length of microtubule.

From this it follows that *the amount of tubulin-t present* at time t at a microtubule end grown from zero length at time zero with constant velocity v_g is, on the average,

$$l_{\mathrm{GTP}}(t)=\int_0^{v_g t} dl\,\chi(l/v_g)$$

$$=l_{\mathrm{GTP}}(\infty)\Phi(t/(\sqrt{2}t_h)), \tag{28}$$

where Φ is the error function and

$$l_{\mathrm{GTP}}(\infty)=\sqrt{\pi/2}v_g t_h. \tag{29}$$

From the properties of the error function it follows that the amount of tubulin-t present at a microtubule end approaches its limit value from below, exponentially fast, and with a characteristic time t_h that is independent of the growth rate. The only dependence on the growth rate is in $l_{\mathrm{GTP}}(\infty)$.

The total amount of tubulin-t at a microtubule end may be compared with the amount in the cap at that end. For this ratio we find

$$l_{\mathrm{GTP}}(\infty)/\langle x\rangle=\sqrt{v_g/v_h}. \tag{30}$$

This ratio typically grows only slowly with v_g since typically $v_g>v_h$.

The number of tubulin-t patches at a microtubule end is, on the average,

$$\begin{aligned}\nu(t)&=\int_0^t dl\, n(l/v_g)\\&=\nu(\infty)\{1-\exp[-(t/t_h)^2/2]\},\end{aligned} \tag{31}$$

where

$$\nu(\infty)=v_g/w_h. \tag{32}$$

This last result is just the steady-state condition for hydrolysis, derived heuristically above with more precision; compare $\nu(\infty)$ with the number of patches in Eq. (10). The difference between Eqs. (10) and (32) arises in the derivation of the latter equation, because it does not take into account the cap's hydrolysis. Consequently, Eq. (10) is the more correct one. Using the values in Table I, Eq. (32) overestimates $\langle n\rangle$ by approximately half a patch for each end. As the number of patches is large in the hydrolysis experiments we shall discuss below, we ignore this difference.

We note that, according to Eqs. (29) and (32), the total amount of tubulin-t at a microtubule end growing with constant velocity v_g is proportional to v_g in the steady state and so is the number of patches it is distributed over. The length of the part of the microtubule containing these patches is also proportional to v_g, as we can see from the form of $\chi(t=l/v_g)$: v_g occurs only in the combination l/v_g in χ.

The number of patches of length x at a microtubule end growing with constant velocity v_g has the following average density with respect to x in the steady state:

$$\begin{aligned}\nu(x,\infty)&=\int_0^\infty dl'\, n(x,l'/v_g)=v_g\int_0^\infty dt'\, n(x,t')\\&=\frac{v_g t_h}{x_h^2}\left\{\sqrt{\frac{\pi}{2}}\left(1+\frac{\xi^2}{2}\right)e^{\xi^2/2}\left[1-\Phi\left(\frac{\xi}{\sqrt{2}}\right)\right]-2\xi\right\},\end{aligned} \tag{33}$$

where ξ is defined in Eq. (F7). $\nu(\infty)$ and $l_{\mathrm{GTP}}(\infty)$, found above, may be derived also from Eq. (33).

Now we can address the questions formulated in Sec. VIII B for the case of microtubules grown from zero length at *constant* tubulin-t concentration and hence with *constant* growth rate v_g. *The rate of GTP hydrolysis* at a microtubule end depends on time as the rate of hydrolysis per patch w_h *times* the number of patches present

$$H(t)=w_h\nu(t)=v_g\{1-\exp[-(t/t_h)^2/2]\}. \tag{34}$$

In this expression the hydrolysis rate is given in lengths of microtubule per unit time. We see that there is an initial lag in the hydrolysis rate relatively to its asymptotic value v_g. GTP-liganded tubulin is associated into the microtubule at a constant rate v_g, but GTP is hydrolyzed at a rate that initially is zero and growing only as t^2. We also note that the rate of hydrolysis approaches its asymptotic rate monotonically and exponentially fast, with characteristic time t_h. Its initial lag is just what is needed to build up the cap and its trailing patches of tubulin-t to their steady-state sizes during constant growth.

We note that this initial lag time is independent of the growth rate v_g and the same for plus ends and minus ends. Thus, for microtubules growing from both ends, the hydrolysis rate per microtubule is obtained by replacing v_g in Eq. (34) by $v_g^{(+)}+v_g^{(-)}$, i.e., with the growth rate of the microtubule. The same substitution applied to Eqs. (28) and (33) gives respectively the amount of GTP present in a microtubule growing from both its end and the number of patches of a given length that this GTP is distributed over.

We conclude that the time required for GTP hydrolysis to reach the fraction y of its steady-state rate v_g is

$$t(y)=\sqrt{-2\ln(1-y)}\,t_h. \tag{35}$$

For example, using the parameter values given in the fourth line of Table I, $t_h=4.8$ s, so $t(95\%)=12$ s and $t(99\%)=15$ s. Thus our model ''predicts'' for hydrolysis experiments that hydrolysis follows microtubule assembly within a few seconds. This agrees with the more recent experimental results [38,39,42] as well as with early results [50,51].

Now suppose we abruptly arrest the growth of a microtubule end that has been growing with constant velocity v_g, while GTP hydrolysis continues with unchanged rates r and w_h. Since tubulin-t is not replenished through growth, we may ask how much time it takes for the tubulin-t at the end to disappear by hydrolysis. The correct way to answer this question consists in solving the master equation (F4) with the distribution given in Eq. (33) as the initial condition. This task is too difficult to be worth the effort. An *upper bound* on the time suffices for our purpose. In order to establish this bound, we note that if the total amount of tubulin-t present $l_{\mathrm{GTP}}(\infty)$ were not already distributed in patches, but instead were present as one continuous stretch of tubulin-t, then it would take *more* time to make it disappear by hydrolysis than it actually does and the relative amount of tubulin-t left at time t after growth was arrested would be $\chi(t)$, given in Eq. (F16), i.e., Eq. (35) describes also an upper bound on the time required for GTP hydrolysis eliminate the fraction y of the GTP present at the time growth from the steady state was arrested.

In conclusion, we have seen that the total amount of tubulin-t present in a microtubule end growing from zero length with constant velocity is a monotonically increasing function of time. Hence, if growth is arrested before the tubulin-t at a growing microtubule end has reached its steady-state value, even smaller amounts of tubulin-t will be found a given time after the arrest than would be found after

arrest from the steady state. We have found an upper bound on the amount of tubulin-t found a given time after arrest from the steady state, expressed in Eq. (35) with $t_h = 4.8$ s, and resulting in at least 99% of the GTP being hydrolyzed 15 s after arrest. This is consistent with recent results [17] that fail to detect any GTP remaining after 15-20 s.

IX. EXPERIMENTS VISUALIZING THE GTP CAP AND MICROTUBULE END STRUCTURE

In a recent elegant experiment a slowly hydrolyzable GTP analog and rhodamine labeled tubulin were used to make caps at ends of microtubules directly observable [19]. These caps are essentially static, their sizes depending only on the time the microtubules were allowed to polymerize in tubulin liganded with the slowly hydrolyzable GTP analog and on the concentration of that tubulin. The experiment serves to illustrate that a cap of tubulin that cannot convert to tubulin-d does stabilize a microtubule made from tubulin-d. Thus the experiment makes it plausible that a short GTP cap will also stabilize such a microtubule. From the cap sizes observed in this experiment, a minimal size for a cap that will stabilize a microtubule is estimated roughly to contain 40 tubulin dimers.

It is in the nature of the model presented in this article that there is no way to define a minimal cap size that will stabilize a growing microtubule. Whatever the growth rate, and hence the average cap size, there is a nonzero catastrophe rate because of the fluctuations in the cap size and hence no absolute stability. We may, however, extract a cap size from our model that is relevant for comparison in a discussion of minimal cap sizes. We know that a microtubule must grow faster than the cap hydrolyzes from its trailing edge for the cap to exist as due to more than a fluctuation. The dimensionless parameter γ parametrizes the relative importance of the various processes contributing to the cap's dynamics; at large-γ values catastrophes are rare and the microtubule is ''stable''; at small-γ values fluctuations dominate. Choosing $\gamma = 1$ as the separator of stabilized microtubules from unstable ones is as good as any other choice we can come up with. This identity corresponds to a value for v_g that is only a fraction larger than v_h. Specifically, we can solve the equation $\gamma = 1$ for v_g and find to a good approximation that

$$v_g / v_h = 1 + 2(r\,\delta x^2 / v_h)^{1/3}, \tag{36}$$

where the last term on the right-hand side is small for the parameter values given in Table I. The value 1 for γ was found sufficiently large to make the large-γ approximation for the catastrophe rate a good approximation. So we assume the same to be true for the cap size and use the expression given in Eq. (E3) for it. This results in

$$\langle x \rangle = \sqrt{\pi}(v_h / r\,\delta x^2)^{1/3}\delta x \quad \text{for} \quad \gamma = 1. \tag{37}$$

Using the parameter values obtained from the fit in Fig. 4 and given in Table I, we find that the ''minimal'' cap contains $\langle x \rangle / \delta x = 26$ tubulin-t dimers.

It cannot be overemphasized that this is a very rough estimate for a number that has no natural definition or meaning within our model. That said, it is close enough to the value 40 reported in [19] to be consistent.

The size of a *typical* cap, on the other hand, is well defined, but depends a little on the velocity of microtubule growth v_g. Using $v_g = 0.75$ μm as a typical value in Fig. 4 and Eq. (E3) with the parameter values determined from that figure, we find $\langle x \rangle = 99\delta x$.

In another recent experiment, the geometrical structure of tips of growing microtubules were studied with cryoelectron micrography and in many cases found to consist of curving sheets of various lengths, some of them long, and apparently containing less than ~ 7 protofilaments [52]. It is in the nature of the coarse-grained modeling done in the present article that nothing can be said about such detailed geometrical structures. We note, however, that if the sheets observed constitute the actual cap, then the sizes observed for these sheets fall in the range of cap sizes predicted by our model for rapidly growing microtubules.

X. EFFECT OF MAGNESIUM ION CONCENTRATION

It has been known for a long time that magnesium promotes microtubule assembly [53–56]. More recent results show that disassembly is promoted as well [57,26,58]. The most recent study measured catastrophe and rescue rates in addition to growth and shrinking rates, varying both the magnesium ion concentration and the tubulin concentration [31]. This makes it interesting to compare our model with the results reported in [31], especially because our model states that the catastrophe rate depends directly on the growth rate, and only indirectly, through the growth rate, on the tubulin concentration. Since the growth rate and the tubulin concentration are proportional, we need to vary something else in order to test this property of our model. Preferably we would like to change the growth rate without changing the tubulin concentration and vice versa. This is where the magnesium ion concentration [Mg] becomes a convenient parameter to vary, since the growth rate v_g increases with [Mg] at fixed tubulin concentration. While convenient, the magnesium ion concentration is no ideal parameter to vary, because, as we shall see, the growth rate is not the only parameter in our model that must depend on [Mg].

In [31], the effect of magnesium ion concentration on the dynamics of individual microtubules was investigated with video-enhanced microscopy for tubulin concentrations varying from 8 to 24 μM. Increasing [Mg] from 0.25 to 6 mM resulted in a (1.5–2)-fold increase in the growth rate $v_g^{(\pm)}$ of both ends, while the shortening rates $v_-^{(\pm)}$ increased by factors 3 and 4–5 for plus and minus ends, respectively. These results are averages, however, as individual microtubules demonstrated individual rates of shortening even during a single phase. Over the concentration range explored, [Mg] significantly affected only the minus end's catastrophe and rescue rates $f_{\rm cat}^{(-)}$ and $f_{\rm resc}^{(-)}$, the higher [Mg] causing more catastrophes and fewer rescues. The catastrophe rate of the plus ends $f_{\rm cat}^{(+)}$ did not depend significantly on the magnesium ion concentration.

The catastrophe rates reported in [31] are given without errors, but must have significant errors judging from the relative distribution of data points in [31], Fig. 5. Since error bars are not given, we cannot make a detailed quantitative comparison between our model and those data. We note, however, that for the largest tubulin-t concentrations shown

in [31], Fig. 5 catastrophe rates for plus and minus ends are equal and independent of magnesium concentration. According to our model, catastrophe rates for plus and minus ends *should* be equal at large tubulin-t concentrations as they cause large growth rates; see Eq. (19). So all that we need is that r is independent of the magnesium concentration and then our model reproduces Fig. 5 in [31] at large tubulin concentration c. From that figure we estimate $f_{\rm cat}^{(\pm)}(c\to\infty)=0.001$–$0.002\ {\rm s}^{-1}$, or 0.06–0.12 $\rm min^{-1}$, in full agreement with the value 0.08 $\rm min^{-1}$ found in Sec. V. This agreement is especially satisfactory because the range of growth rates $v_g^{(+)}$ used in the fit in Sec. V is 0.2–1 μm/min, while the values of $v_g^{(+)}$ and $v_g^{(-)}$ corresponding to the largest tubulin-t concentrations in Fig. 5 in [31] are 4 μm/min and 2μm/min, respectively.

In Fig. 5 in [31], $f_{\rm cat}^{(+)}$ barely depends on the magnesium concentration and $f_{\rm cat}^{(-)}$ at [Mg] = 6 mM seems equal to $f_{\rm cat}^{(+)}$. Since we have already seen that r is independent of [Mg], the [Mg] independence of $f_{\rm cat}^{(+)}$ implies that $v_h^{(+)}$ grows with [Mg] like $v_g^{(+)}$ does, i.e., the ratio $v_h^{(+)}/v_g^{(+)}$ is independent of [Mg]. The identity of $f_{\rm cat}^{(-)}$ at [Mg] = 6 mM with $f_{\rm cat}^{(+)}$ implies $v_h^{(-)}/v_g^{(-)}=v_h^{(+)}/v_g^{(+)}$ for any tubulin-t concentration at [Mg] = 6 mM.

The apparent independence of tubulin-t concentration demonstrated by $f_{\rm cat}^{(-)}$ at [Mg] = 0.25 mM in [31], Fig. 5, is easily reproduced by our model: it only requires that $v_h^{(-)}\ll v_g^{(-)}$ for the growth rates $v_g^{(-)}$ corresponding to the tubulin-t concentrations 8–16 μM in [31], Fig. 5, i.e., for $v_g^{(-)}$ = 0.7–4 μm/min according to [31], Fig. 1. We found in Sec. IV that $v_h^{(-)}$ is about a factor 2 smaller than $v_h^{(+)}$, which was found to be equal to 0.2 μm/min at 1mM [Mg] in Sec. V. So we expect $v_h^{(-)}$ to be less than 0.1 μm/min, in full agreement with the condition $v_h^{(-)}\ll v_g^{(-)}=0.7$ μm/min. In conclusion, our model seems quite able to reproduce the dependence of $f_{\rm cat}^{(\pm)}$ on both the tubulin-t concentration and magnesium concentration.

XI. EFFECT OF MAPS

Microtubule associated proteins (MAPs), such as τ [13], XMAP215 [59,60], and XMAP230 [61], provide, like magnesium ions, a means for changing the growth rate without changing the tubulin concentration. This gives us an opportunity to compare catastrophe rates obtained at the same growth rate, but with different concentrations of tubulin (and τ). It is, of course, not obvious that we should be able to learn anything about our model from experiments done in the presence of MAPs. After all, the model was designed to describe the cap dynamics of a pure-tubulin microtubule. MAPs are proteins attaching themselves to microtubules, thereby changing their dynamics. Only if these changes can be described by a change of parameter values in our model will the model be able to describe the effect of MAPs.

A quantitative study of the effect of τ on growth, catastrophe, and shrinking rates of plus ends was reported in [13]. Our model gives the catastrophe rate as a function of the growth rate. So the measurements reported in [13] for those two rates provide us with a possibility to test the model.

Figure 5 in [13] shows that as the concentration of τ is increased from zero to 1μM, the growth rate $v_g^{(+)}$ is increased by a factor 3. If this increase in $v_g^{(+)}$ were the only effect of τ, a plot of the catastrophe rate against the growth rate should look the same no matter what combination of tubulin-t and τ concentrations is responsible for any given growth rate. Such a plot is given in [13], Fig. 7(B), which shows that the catastrophe rate at a given growth rate is reduced by at least a factor 4 by the increase of τ concentration from zero to 1μM.

Comparing the asymptotic value of $f_{\rm cat}$ at large growth rate given in Eq. (19) with [13], Fig. 7(B), we see that 1 μM τ must have reduced the interior hydrolysis rate of the cap r significantly. In [13] an upper bound of $0.002\ {\rm s}^{-1}$ is given for the asymptotic value of $f_{\rm cat}^{(+)}$ at large growth rates. Thus, if our model is to describe the effect of τ, the presence of 1μM τ reduces r by at least a factor 7 compared to the value of r we determined in Sec. V. The catastrophe rates given for lower tubulin-t concentrations in [13], Fig. 7(B) indicate that $v_{\rm h}^{(+)}$ is reduced from 0.2 μm/min to $\sim$0.1μm/min by the presence of 1μM τ, while r is reduced only by a factor 4. All things considered, the difference between factors 4 and 7 is hardly significant.

The abrupt decrease of $f_{\rm cat}^{(+)}$ to zero with increased τ concentration reported in [13], Fig. 7(C) can be understood from our expression in Eq. (19): Increasing the τ concentration simultaneously reduces r and $v_h^{(+)}$ and increases $v_g^{(+)}$, all three changes serving to reduce the catastrophe rate. Similar considerations can be applied to the effects of XMAP215 [59,60] and XMAP230 [61].

XII. DISTRIBUTION OF CATASTROPHE TIMES

Our model predicts more than just the average catstrophe rate: It also predicts the distribution of catastrophe times. While the exact distribution is somewhat complicated, in the experimentally relevant case $\gamma>1$ the model predicts [see Eq. (D2)] that the distribution should be very nearly exponential. This prediction has been tested by recent experiments [18]. These authors find that the distribution for the minus end is indistinguishable from an exponential, while the plus end is nonexponential with a confidence of 97%. There are fewer short-time events than one would expect from an exponential distribution.

These data suggest that there are measurable limits to the accuracy of the model presented here. Given the number of simplifications in the model, we do not find this surprising. The fact that their data are so nearly exponential (see [19] Fig. 2), can be taken as further support of the basic principles of the model. Deviations may represent corrections to our coarse-grained picture. Or the data set analyzed in [19] may actually be exponentially distributed: The result of the statistical test only states that it *probably* is not.

Other results [62] in *Xenopus laevis* egg extracts show that the distribution of catastrophe times in extracts is nonexponential. These extracts, however, contain many of the components of living cells and one knows that the microtubule dynamics can be extensively modified [27]. Therefore, these experiments do not directly tell us about the mechanism of dynamic instability in purified tubulin.

XIII. UV CUTTING EXPERIMENTS

Any cap model predicts that if the cap is lost, a microtubule has a catastrophe. An experiment [20] to directly test this hypothesis yielded an interesting result. The authors used an UV microbeam to cut off the end of growing microtubules. The exposed plus end always (16 out of 16 times) suffered a catastrophe, as one would expect from a cap model. However, the exposed minus end always (29 out of 29 times) continued elongating. If these results are not artifactual, then they show that the dynamics of the minus end are fundamentally different from those of the plus end and it may not be possible to model them in a combined fashion as done here.

There are several caveats to the interpretation of this experiment. First of all, the results are sensitive to the buffer conditions: If the magnesium concentration is raised, then a significant number of minus-end catastrophes are observed [63]. It is possible that the microtubules are photodamaged by the UV microbeam and that this damage determines the outcome of the experiment. One also does not know whether the continued growth of the minus end should be attributed to the lack of a catastrophe or to the occurrence of a rescue [5], a discussion made difficult by our ignorance about the mechanism of rescue. Nevertheless, these experiments point to the possibility that there are important differences between the two ends. We hope that further experiments will pursue this issue.

XIV. DISCUSSION

A. Self-consistency of the model

It was assumed in the formulation of the model, at the stage where we got rid of the microscopic description, that $k_h' \ll k_h$. Now that the model parameters have been determined by fitting the model to experimental results, this criterion must be satisfied, or the model is not self-consistent. We find, using parameter values from the first line in Table I, that

$$k_h'/k_h = r\,\delta x^2/v_h = 3\times 10^{-4}, \tag{38}$$

which shows that k_h' indeed is much smaller than k_h.

B. Microscopic interpretations of the model

We have presented this model in terms of a *hydrolysis cap*. It is important to realize that the model is in fact far more general than this and can be used to describe a number of microscopic models. Some examples are the following.

1. Conformational or lattice shift cap

Tubulin units assemble in one conformational state or lattice configuration, but later (after hydrolysis?) shift to a second conformation. This shift can occur in two ways: (i) *induced shift*, in which the conformational change in one region is catalyzed because a neighboring region is in the second conformational state, and (ii) *spontaneous shift*, in which a region spontaneously changes state.

2. Protofilament cap

Recent results [52] indicate that growing microtubules possess a sheet of protofilaments that are not bound together into a tube. This suggests a possible model in which a catastrophe occurs when the sheet vanishes. The unbound protofilaments become longer as the microtubule grows, but they may bind to each other by two mechanisms: (i) *zippering*, in which the tube state is propagated forward, and (ii) *spontaneous binding*, in which protofilaments bind to each other somewhere in the middle of the sheet.

3. MAP-free cap

In this model, catastrophes are caused by a catastrophe-inducing MAP reaching the tip of a growing microtubule. These MAPs crawl forward along on the microtubule towards the tip, which recedes from them as the microtubule grows. New MAPs may bind anywhere along the length of the microtubule. The MAP-free region at the growing tip of a microtubule may be shortened by two mechanisms, either the forward progress of an already-bound MAP or by the binding of a new MAP somewhere within the MAP-free region. It is of interest to note that motor proteins that increase the catastrophe rate have recently been discovered [64].

These examples that help illustrate that the basic ingredients of the model are the following:

(i) Growing microtubules possess a cap, the disappearance of which leads to a catastrophe and (ii) the cap is lengthened by the growth of the microtubule and shortened by two mechanisms: *front propagation* and *spontaneous events*. Spontaneous events become more likely as the cap becomes longer. Any microscopic model that leads to these phenomena can be described in terms of a model similar to the one we propose.

C. Rescues

We propose that when the loss of the cap causes disassembly from the end of the MT and disassembly reaches a left-behind patch of tubulin-t, it continues right through it. This implies the existence of additional elements of the dynamics, e.g., GTP hydrolysis is propagated in front of the disassembling tip. The reversal of disassembly to assembly, called *rescue*, thus requires something more than a leftover patch of tubulin-t, according to our model.

Previous models [12,11] have considered rescues and catastrophes to be two aspects of the same phenomenon. However, we feel that there is little evidence to suggest that this is the case. Indeed, the fact that the rescue rate may be ''adjusted'' independently of the catastrophe rate under some conditions [26–28] could be taken as evidence that the two phenomena arise from different mechanisms. Others [4] have also suggested this possibility.

One could build a model for rescues as well. We have refrained from doing this for a simple reason: Much less data has been collected on rescues than on catastrophes. We hope that future experiments will address this aspect.

D. Issues for future experiments

We expect that video microscopy will continue to provide the data that most constrain models of dynamic instability. It

would be very useful to have the catastrophe rate and dilution experiments repeated under identical conditions. Recent gains in understanding the effect of buffer conditions [33–35] may offer new experimental possibilities. By measuring growth velocity, catastrophe rate, and lifetime upon dilution for a variety of tubulin concentrations, the major parameters of our model (growth velocity and off rate [23–25], v_h, and r) would be *overdetermined*, thus providing a rigorous test of the model.

The combination of video microscopy with *pressure jump* experiments [65,66] has not been exploited. It should be feasible to construct a pressure cell that permits continuous viewing of individual microtubules [67]. Pressure offers an extremely attractive alternative to dilution because it can be adjusted rapidly and with high precision. Our model makes a specific prediction: The stabilizing cap should equilibrate to the new pressure in an average time $t_{\rm cat}$, given by Eq. (25). For times shorter than $t_{\rm cat}$, a ''memory'' of the previous state persists; the speed with which pressure can be controlled should make this time scale easily accessible.

Finally, the heterogeneity that one sees in the growth velocities of a population of MTs [68] is still not completely understood. It may be profitable to try to correlate the variability in growth velocity with the occurrence of catastrophes. For example, do MTs that grow more rapidly have less frequent catastrophes? Or is an individual MT more likely to have a catastrophe during periods when its growth is particularly slow (or fast)? These experiments should not require any new apparatus or procedures.

ACKNOWLEDGMENTS

We have benefited from discussions with Denis Chrétien, Marileen Dogterom, David Drechsel, Deborah Fygenson, Eric Karsenti, Albert Libchaber, David Odde, and Rich Walker. H. F. was partially supported by the Danish Natural Science Research Council, Grant No. 11-0244-1, and by Julie Damm's Studiefond. T. H. would like to thank AT&T for financial support. We also acknowledge partial support by the NSF (Grant No. PHY-9408905), the NIH (Grant No. GM50712), and Human Frontiers Science Project.

APPENDIX A: NOTATION

This appendix collects our notation, which was introduced gradually throughout the article wherever needed for the first time. Notation not used more than once in the article is not included. t denotes time. x is the length of the GTP cap. $\delta x = 0.6$nm is the amount by which the length of a microtubule and its GTP cap is incremented by the addition of one heterodimer to it. δx is also the amount by which the cap and trailing patches of GTP shorten by hydrolysis of one heterodimer. k_g is the rate heterodimers are added to a growing microtubule end. $v_g = k_g \delta x$ is the average velocity of growth resulting from the rate k_g. $v_g^{(+)}$ and $v_g^{(-)}$ are the notations used when we wish to distinguish between the two ends' velocities of growth. k_h is the rate of hydrolysis for heterodimers at the trailing edge of the cap or at the edge of GTP patches. $v_h = k_h \delta x$ is the velocity with which these edges, or hydrolysis fronts, propagate. $v_h^{(+)}$ and $v_h^{(-)}$ are the notations used when we wish to distinguish the two different orientations possible for a hydrolysis front. $v = v_g - v_h$ is the velocity with which the cap grows. It is also the velocity with which it grows before dilution, in dilution experiments, while v' is its growth velocity after dilution. D is the diffusion constant parametrizing the unbiased random walk performed by $x - vt$ in time intervals between cutting by internal hydrolysis. Its value is given in Eq. (6). k_h' is the rate of hydrolysis for hetero-dimers in the interior of the cap or a GTP patch. $r = k_h'/\delta x$ is the rate per unit length cap or patch that interior hydrolysis opens up two new hydrolysis fronts. $w_h = v_h^{(+)} + v_h^{(-)}$ is the velocity with which a GTP patch shrinks. γ is a dimensionless parameter characterizing the dynamics of the cap, defined in Eq. (15). $f_{\rm cat}$ is the catastrophe rate. $t_{\rm cat}$ is the average waiting time for dilution-induced catastrophes, defined in Eq. (25). $p_{\rm cat}(t)$ is the waiting-time distribution for dilution induced catastrophes. $l_{\rm GTP}$ is the amount of GTP at a microtubule end, measured in lengths of microtubule. χ is the amount of GTP per unit length of microtubule at a given time for a homogeneous microtubule and at a given position for an inhomogeneous one. $\nu(x,t)$ is the average number of GTP patches of length x per unit length microtubule at time t. $t_h = (r w_h)^{-1/2}$ is the characteristic time for hydrolysis processes, defined in Eq. (23). $x_h = (w_h/r)^{1/2}$ is the characteristic length of GTP patches in hydrolysis, defined in Eq. (F6).

APPENDIX B: MASTER EQUATION

The evolution in time of an ensemble of microtubule caps evolving according to the dynamics described in Sec. III is described by a linear master equation

$$\partial_t p(x,t) = -\partial_x j(x,t), \tag{B1}$$

where

$$j(x,t) = v p(x,t) - D \partial_x p(x,t) - r x P(x,t). \tag{B2}$$

Here $p(x,t)$ is the ensemble density of microtubules with caps of length x at time t, and we have introduced the number

$$P(x,t) = \int_x^\infty dx' p(x',t) \tag{B3}$$

of microtubules with caps of length longer than x.

$P(0,t)$ is the total number of microtubules with caps at time t. It satisfies the equation

$$\partial_t P(0,t) = j(0,t) = v p(0,t) - D \partial_x p(0,t), \tag{B4}$$

which shows how the number of capped microtubules evolves in time: it decreases at the rate $D \partial_x p(0,t)$ with which caps are lost by diffusion to vanishing length and, for $v > 0$, increases at the rate $v p(0,t)$, if by some mechanism we supply the ensemble with new, growing microtubules with caps of zero length. For $v < 0$, the term $v p(0,t)$ describes loss of caps by convection to vanishing length. Because $p(x,t) = 0$ for $x < 0$, the diffusive loss of caps will be infinite if $p(0^+,t) > 0$, thereby forcing the system to obey the boundary condition $p(0^+,t) = 0$ whenever it is left to itself.

In that situation, the *catastrophe rate* f_{cat}, the rate per capped microtubule at which caps are lost, is

$$f_{\mathrm{cat}} = D\partial_x p(0,t)/P(0,t). \tag{B5}$$

We see that Eqs. (39) and (40) contain a total of three parameters v, D, and r. These are the fundamental parameters of our model, which is an effective theory with only D/v relating to the microscopic scale.

The description given here in terms of a master equation is not the only one possible. One can, alternatively, describe the time evolution of the cap by a Langevin equation with a velocity v and two noise terms, one for the fluctuations in velocity and another for the cutting by internal hydrolysis. But for the purposes of the present article we find the master equation more convenient.

APPENDIX C: RIGOROUS ANALYSIS OF MODEL—GENERAL RESULTS

Equations (B1) and (B2) comprise an integro-differential equation for $p(x,t)$. Differentiating it once with respect to x makes it a third-order partial differential equation for $p(x,t)$. Fortunately, we do not have to deal with these equations. Instead we integrate Eq. (B1) with respect to x from x to infinity and find

$$\partial_t P(x,t) = j(x,t) = (-v\partial_x + D\partial_x^2 - r x)P(x,t), \tag{C1}$$

where we have assumed $j(\infty,t)=0$ for all t. This boundary condition is satisfied as long as $p(x,t)$ decreases faster than x^{-2} at infinity. The opposite case makes the average cap length infinite, a state that is impossible to arrive at with the dynamics of this model, as long as caps are created with finite length.

The three dimension-full parameters v, D, and r in Eq. (C1) can be combined to form three other independent parameters, of dimension length, time, and none, corresponding to the dimensions of Eq. (C1)'s two dependent variables:

$$x_0 \equiv (D/r)^{1/3}, \tag{C2}$$

$$t_0 \equiv (Dr^2)^{-1/3}, \tag{C3}$$

$$\gamma \equiv \frac{v}{2D^{2/3}r^{1/3}} = \frac{v}{2x_0/t_0}. \tag{C4}$$

The inverse relations to Eqs. (C2) and (C3) are illustrative and useful,

$$D = x_0^2/t_0, \tag{C5}$$

$$r = (x_0 t_0)^{-1}. \tag{C6}$$

Introducing new, dimensionless variables

$$\xi \equiv x/x_0, \tag{C7}$$

$$\tau \equiv t/t_0, \tag{C8}$$

$$\widetilde{P}(\xi,\tau) \equiv \exp[-vx/(2D)]P(x,t) \tag{C9}$$

in Eq. (C1), it reads

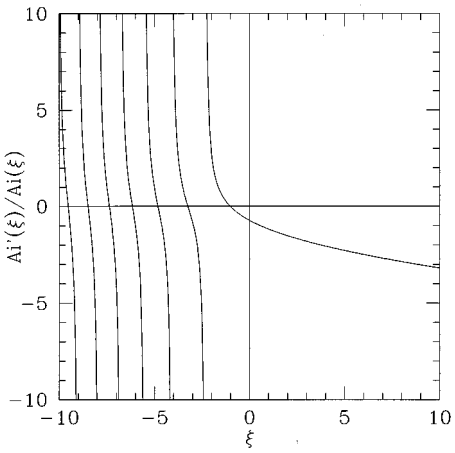

FIG. 7. Graph of $\mathrm{Ai}'(\xi)/\mathrm{Ai}(\xi)$. With this graph one may solve Eq. (C13) graphically.

$$\partial_\tau \widetilde{P}(\xi,\tau) = (\partial_\xi^2 - \xi - \gamma^2)\widetilde{P}(x,t). \tag{C10}$$

The general solution to this linear equation is

$$\widetilde{P}(\xi,\tau) = \int d\alpha\, c(\alpha)\exp(-\alpha\tau)\mathrm{Ai}(\xi+\gamma^2-\alpha), \tag{C11}$$

where $\mathrm{Ai}(\xi)$ is the first Airy function, satisfying Airy's differential equation (see [69], Chap. 10)

$$\left(\frac{d^2}{d\xi^2} - \xi\right)\mathrm{Ai}(\xi) = 0. \tag{C12}$$

The second Airy function $\mathrm{Bi}(\xi)$ is eliminated from the general solution by its exponential growth at infinity.

Different boundary conditions at $x=0$ put different constraints on the coefficient function $c(\alpha)$ in Eq. (C11). Suppose we leave the ensemble of caps to itself for $t>0$. Then $p(0,t)=0$ for all $t>0$ and consequently $c(\alpha)$ is nonzero only for the discrete set of values α_k, $k=0,1,2,\ldots$, satisfying

$$\frac{-\mathrm{Ai}'(\gamma^2-\alpha_k)}{\mathrm{Ai}(\gamma^2-\alpha_k)} = \gamma. \tag{C13}$$

This equation defines α_k as implicit functions of γ as illustrated in Fig. 7. We have determined several of these functions numerically. The graphs of the first 18 functions are shown in Fig. 8. For any value of γ,

$$\alpha_k \sim \gamma^2 + \left(\frac{3}{2}\pi k\right)^{2/3} \quad \text{for } k\to\infty. \tag{C14}$$

For any positive value of γ^2, the set of functions $\mathrm{Ai}[\xi+\gamma^2-\alpha_k(\gamma)]$, $k=0,1,2,\ldots$, form a basis for real functions on the real positive-ξ axis. This basis is orthogonal in the scalar product

$$\langle f,g\rangle \equiv \int_0^\infty d\xi\, f(\xi)g(\xi) \tag{C15}$$

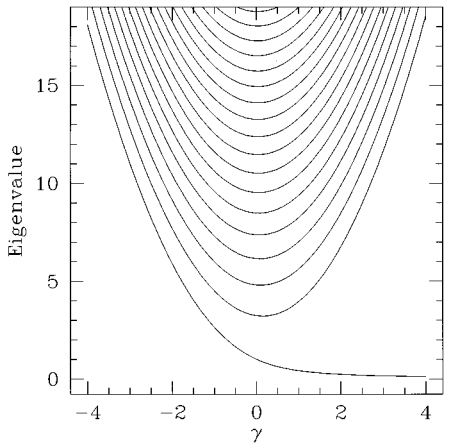

FIG. 8. Graphs of $\alpha_k(\gamma)$ for $k=0,1,2,\ldots$, counting up from the bottom. Note the gap between $\alpha_0(\gamma)$ and $\alpha_k(\gamma)$, $k=1,2,\ldots$, for $\gamma \geqslant 1$. It is the reason why the term with $k=0$ quickly dominates the sum over k in Eqs. (C18) and (C19) as τ increases from zero.

and one can show that the kth function has norm $\sqrt{\alpha_k}\mathrm{Ai}(\gamma^2-\alpha_k)$. With this knowledge, we can find the time evolution for a particularly interesting initial situation, the one in which all cap lengths are zero at time $t=0$. This condition is described by setting

$$p(x,0) \propto -\delta'(x) \tag{C16}$$

or, equivalently,

$$P(x,0) \propto \delta(x). \tag{C17}$$

This initial condition results in

$$P(x,t) \propto \sum_{k=0}^{\infty} \exp(-\alpha_k \tau + \gamma\xi) \frac{\mathrm{Ai}(\xi+\gamma^2-\alpha_k)}{\alpha_k \mathrm{Ai}(\gamma^2-\alpha_k)}, \tag{C18}$$

where ξ and τ are related to x and t by Eqs. (C7) and (C8).

From Eqs. (C18) and (B3) it follows that

$$p(x,t) \propto x_0^{-1} \sum_{k=0}^{\infty} \exp(-\alpha_k \tau + \gamma\xi) \times \frac{-\mathrm{Ai}'(\xi+\gamma^2-\alpha_k) - \gamma \mathrm{Ai}(\xi+\gamma^2-\alpha_k)}{\alpha_k \mathrm{Ai}(\gamma^2-\alpha_k)}. \tag{C19}$$

Phrased differently, Eq. (C19) gives the propagator for caps starting out with zero length. Since $P(0,t)$ is the total number of caps in the ensemble, we see that this number is *infinite* at time $t=0$ according to Eq. (C17), but finite at any later time according to Eq. (C18). Because caps disappear from the ensemble by diffusion through $\xi=0$ and we start the caps out with a vanishing ξ value, we must have an infinite number of caps in the ensemble initially for a finite number of caps to survive to any later time.

This infinity is an artifact of our continuum description. As we will not have to deal with early times, we will not encounter it. It is not different from what one finds for ordinary diffusion on the real positive axis with a source and a sink at the origin. The reason it is not different is that at very short length scales, such as in the immediate neighborhood of the origin, the diffusion term dominates over the other terms in our master equation.

APPENDIX D: CATASTROPHE RATE

As argued in Sec. V, caps on the *observed* microtubules have existed for a sufficiently long time for the ensemble of them to be statistically distributed as the asymptotic distribution obtained from Eq. (C18) for $\tau \to \infty$, i.e., as

$$P(x,t) \propto \exp(-\alpha_0 \tau + \gamma\xi)\mathrm{Ai}(\xi+\gamma^2-\alpha_0). \tag{D1}$$

Since

$$P(0,t) \propto \exp(-\alpha_0 \tau) \tag{D2}$$

is the total number of caps in such an ensemble, the catastrophe rate obviously is

$$f_{\mathrm{cat}} = \alpha_0 / t_0 . \tag{D3}$$

Here α_0 is a function of γ. Its graph is shown as the lowest curve in Fig. 8. Notice that this lowest curve for positive values of γ is well below the other curves shown. This means that neglecting terms with $k>0$ in Eq. (C18), as we do with Eqs. (D1)–(D3), is a good approximation even for moderate values of τ.

Furthermore, the first term in the asymptotic expansion of $\alpha(\gamma)$ in terms of $1/\gamma$ gives a very good approximation already for $\gamma>1$, because the second term in the expansion has coefficient zero

$$\alpha_0 = \frac{1}{2\gamma} + O\left(\frac{1}{\gamma^3}\right). \tag{D4}$$

Using this and Eqs. (C3) and (C4), we obtain

$$f_{\mathrm{cat}} = Dr/v + O\left(\frac{1}{\gamma^3}\right), \tag{D5}$$

from which we see that the heuristic result given in Eq. (19) for large values of γ actually is correct as an approximation and is a very good one: compare the full and dashed curves in Fig. 4. Figure 4 shows a fit based on the full expression in Eq. (C18) including terms with $k>0$. Because of these terms with $k>0$, the instantaneous catastrophe rate

$$f_{\mathrm{cat}}(t) = \frac{dP(0,t)}{dt} \Big/ P(0,t) \tag{D6}$$

is time dependent, being larger initially than its asymptotic value, which is approached monotonically. We calculated the average time that a microtubule is observed in its growing state as

$$\langle t \rangle = P(0,t_{\mathrm{cutoff}})^{-1} \int_{t_{\mathrm{cutoff}}}^{\infty} dt (t - t_{\mathrm{cutoff}}) \left| \frac{dP(0,t)}{dt} \right| = P(0,t_{\mathrm{cutoff}})^{-1} \int_{t_{\mathrm{cutoff}}}^{\infty} dt\, P(0,t). \tag{D7}$$

Here t_{cutoff} is the time it takes microtubules to grow long enough to be observed, i.e., $t_{\text{cutoff}}=x_{\text{cutoff}}/v_g$, where x_{cutoff} is the minimal length that a microtubule needs to have to be observed. We have used $x_{\text{cutoff}}=0.1\mu\text{m}$ as this is the typical resolution of the light microscopes used to take the data.

For any nonzero value for t_{cutoff}, Eq. (D7) is the observed average lifetime of microtubules, related to the observed catastrophe rate by

$$f_{\text{cat}}=1/\langle t\rangle. \tag{D8}$$

The limit $t_{\text{cutoff}}\rightarrow 0$ is tricky. The exact expression for the observed catastrophe rate given in Eq. (D8) is the one our model tells us to use in the limit of $t_{\text{cutoff}}\rightarrow 0$. This catastrophe rate is infinite, because with the particular choice of initial condition leading to Eq. (C18), $\langle t\rangle$ vanishes with t_{cutoff} in Eq. (D7). This is so because an infinity of microtubules vanish in the first instant after they are created with zero length at $t=0$, while only a finite number survive a finite time, as discussed in the last two paragraphs of Appendix C. As also explained there, this infinity is an artifact of our continuum description of the cap and is an acceptable artifact since it only shows up in situations that are not encountered when we relate to experimental data, while the continuum description greatly facilitates our modeling task.

APPENDIX E: DILUTION EXPERIMENTS

Our model is a partial differential equation, and initial data and boundary conditions characterizing dilution experiments are required in order to describe such experiments with the model. We meet this requirement in the following way. When microtubules are grown at high tubulin concentration, catastrophes are very rare, so the caps on such microtubules are as old as the microtubules themselves. When these microtubules are grown from seeds, i.e., from zero length, each cap has aggregated and lost again by hydrolysis as much tubulin-t as there is tubulin in the microtubule. So the ensemble of caps in an ensemble of such microtubules is extremely well equilibrated statistically, i.e., distributed according to the asymptotic form given in Eq. (D1). When the growth rate v_g is so large that $\gamma^2\gg 1$, $\gamma>0$, the right-hand side of Eq. (D1) is well approximated by the first term in its expansion in γ^{-2},

$$\begin{aligned}P(x,0)&=\exp(\gamma\xi)\frac{\text{Ai}(\xi+\gamma^2-\alpha_0)}{\text{Ai}(\gamma^2-\alpha_0)}\\&=\exp\left(-\frac{\xi^2}{4\gamma}\right)+O(\gamma^{-2}).\end{aligned} \tag{E1}$$

Alternatively, we may arrive at the last expression in Eq. (E1) by neglecting the diffusive term in our master equation (C1), that is, by setting $D=0$ in it. Then the steady-state solution to the master equation is easily found to be the last expression on the right-hand side of Eq. (E1). Either way, this approximation results in the steady-state distribution

$$p(x)=\frac{rx}{v}\exp\left(-\frac{rx^2}{2v}\right), \tag{E2}$$

with mean value

$$\langle x\rangle=\sqrt{\frac{\pi v}{2r}}. \tag{E3}$$

Comparing this result with our estimate in Eq. (13), we see that the latter is very good: it has the form we expected from dimensional analysis and only misses the numerical prefactor by a factor $\sqrt{\pi}/\sqrt{3}=1.02$. Considering the method of estimation, this precision is the result of luck.

Though we have neglected the diffusive term responsible for catastrophes by assuming $D=0$ in deriving the distribution (E2), we can still find the catastrophe rate that results from this distribution when catastrophes are permitted by having D nonzero. Strictly treated, these catastrophes will affect the form of the distribution, but that is a higher-order effect in D that can be ignored to a good approximation when D is small. The catastrophe rate is

$$f_{\text{cat}}=D\left.\frac{dp}{dx}\right|_{x=0}=\frac{Dr}{v}, \tag{E4}$$

which is just what one gets from inserting Eq. (D4) into Eq. (D3). So now we also understand that approximate result as a leading-order perturbative result.

Exact or approximated, the function (E1) is our initial data for the cap length distribution when we model dilution experiments. Suppose that the tubulin concentration c at which microtubules are grown is diluted abruptly to concentration c' at time $t=0$. Then, with primes denoting values for $t>0$, the cap length distribution evolves according to

$$\begin{aligned}P(x,t)=\sum_{k=0}^{\infty}c_k(\gamma,\gamma')&\exp(-\alpha_k'\tau'+\gamma'\xi')\\&\times\frac{\text{Ai}(\xi'+\gamma'^2-\alpha_k')}{\sqrt{\alpha_k'}\text{Ai}(\gamma'^2-\alpha_k')},\end{aligned} \tag{E5}$$

where

$$\begin{aligned}c_k(\gamma,\gamma')=\int_0^{\infty}d\xi'&\frac{\text{Ai}(\xi'+\gamma'^2-\alpha_k')}{\sqrt{\alpha_k'}\text{Ai}(\gamma'^2-\alpha_k')}\\&\times\exp[(\gamma x_0'/x_0-\gamma')\xi']\frac{\text{Ai}(\xi' x_0'/x_0+\gamma^2-\alpha_0)}{\text{Ai}(\gamma^2-\alpha_0)}\end{aligned} \tag{E6}$$

is the scalar product [Eq. (C15)] between our diagonalizing basis vectors for $t>0$ and our initial condition at $t=0$.

The distribution in time of catastrophes following dilution is the instantaneous rate at which caps disappear from the ensemble of caps we had at the time of dilution $t=0$:

$$p_{\text{cat}}(t)=-\partial_t P(0,t)/P(0,0). \tag{E7}$$

For the average lifetime of caps following dilution we then have

$$t_{\rm cat}=\int_0^\infty dt\, t p_{\rm cat}(t)$$
$$=t_0'\sum_{k=0}^{\infty}\alpha_k'^{-3/2}c_k(\gamma,\gamma')\Big/\sum_{k=0}^{\infty}\alpha_k'^{-1/2}c_k(\gamma,\gamma'). \tag{E8}$$

For only slight dilution, $\gamma'\simeq\gamma$ and the exact expressions in Eqs. (E5) and (E8) are well approximated by the first, or the first few, terms in the sum over k. For the more interesting case of massive dilution, $\gamma'\sim 0$ or $\gamma'<0$ and many terms are required in the sums in Eqs. (E5) and (E8) to obtain a reasonable approximation. Also, little is gained by using the approximation of Eq. (E1) in Eq. (E6). However, for $v'<0$ cap ''growth'' is negative and causes cap loss by the convective term in Eq. (C1) in addition to the loss by its diffusive term. In this case we can neglect the diffusive term to a good approximation for $|\gamma|$ large, as it only causes a slight smearing of the cap-lifetime distribution obtained without it. Setting $D=0$ in Eq. (C1), we can solve it exactly for $t>0$ by using the method of characteristic lines and find

$$P(x,t)=\exp(-rxt+\tfrac{1}{2}rv't^2)P(x-v't,0). \tag{E9}$$

We could improve on this approximate result by treating it as a leading-order approximation in a perturbation theory in D, but do not need to for our purposes here.

So now we know the cap length distribution at all times after dilution to a concentration that renders v' sufficiently negative,

$$P(x,t)=\exp(-rxt+rv't^2/2)\frac{\mathrm{Ai}\left(\dfrac{x-v't}{x_0}+\gamma^2-\alpha_0\right)}{\mathrm{Ai}(\gamma^2-\alpha_0)}$$
$$=\exp[(1-v'/v)(rv't^2/2-rxt)-rx^2/(2v)]$$
$$+O(\gamma^{-2}). \tag{E10}$$

Notice the normalization $P(0,0)=1$. $P(0,t)$ is the fraction of microtubules that have not yet experienced catastrophe at time t after dilution and is just a Gaussian distribution to leading order in γ^{-2}. So, then, is the distribution in time of catastrophes

$$p_{\rm cat}(t)=-\partial_t P(0,t)=\frac{\pi t}{2t_{\rm cat}^2}\exp\left(-\frac{\pi t^2}{4t_{\rm cat}^2}\right), \tag{E11}$$

where the average lifetime upon dilution is

$$t_{\rm cat}=\left[\frac{-2rv'}{\pi}\left(1-\frac{v'}{v}\right)\right]^{-1/2}\simeq\left(\frac{\pi}{-2rv'}\right)^{1/2} \tag{E12}$$

in the approximation used here.

APPENDIX F: GTP HYDROLYSIS RATES—CASE OF HOMOGENEOUS MICROTUBULE

The variables needed to describe the kinetics of GTP hydrolysis are well illustrated by a much simplified situation. From their functional forms in this situation we easily obtain their forms in realistic situations in Sec. VIII C and in Appendix G.

We consider an infinitely long microtubule that at time $t=0$ consists entirely of tubulin-t. After that time it suffers internal hydrolysis at rate r per unit length, and hydrolysis from the ends of the patches thus created, each patch shrinking with velocity $w_h=v_h^{(+)}+v_h^{(-)}$. Let $n(x,t)$ denote the average number of patches of length x to be found per unit length of microtubule at time $t\geq 0$; since this is an average, it is a real number. The total number of patches per unit length of microtubule then is

$$n(t)\equiv\int_0^\infty dx\, n(x,t). \tag{F1}$$

Similarly, the total length of tubulin-t per unit length of microtubule is

$$\chi(t)\equiv\int_0^\infty dx x n(x,t) \tag{F2}$$

at time t and should equal 1 at time $t=0$. The average length of patches at time t is

$$\langle x\rangle_t=\chi(t)/n(t). \tag{F3}$$

The density $n(x,t)$ evolves in time according to the master equation

$$\partial_t n(x,t)=w_h\partial_x n(x,t)-rxn(x,t)+2r\int_x^\infty dx' n(x',t). \tag{F4}$$

On the right-hand side of this integro-differential equation, the first term describes the change of patch length by hydrolysis from both ends at velocity $w_h=v_h^{(+)}+v_h^{(-)}$. The second term describes the loss of patches of length x caused by their internal hydrolysis at rate rx. The third term describes the creation of patches of length x from patches of any length $x'>x$ by internal hydrolysis at rate r per unit length. The factor 2 in front of this term is there because one event of internal hydrolysis in a patch of length x' can create a patch of length x in two ways: by separating the length x either from one end or from the other end.

The master equation (F4) contains two parameter r and w_h with dimensions [length $\times$ time]$^{-1}$ and [length/time], respectively. These parameters may be replaced by two other parameters

$$t_h\equiv(rw_h)^{-1/2} \tag{F5}$$

and

$$x_h\equiv(w_h/r)^{1/2} \tag{F6}$$

of dimensions (time) and (length), respectively. The latter parameters define the time and length scales of the process of hydrolysis. t_h was introduced already in Eq. (23). Using the values for r and $v_h^{(\pm)}$ given in Table I, we find $t_h=5$ sec and $x_h=29$ nm. When time and length are measured in units of these parameters,

$$\xi \equiv x/x_h, \tag{F7}$$

$$\tau \equiv t/t_h, \tag{F8}$$

$$\tilde{n}(\xi,\tau) \equiv x_h^2 n(x,t) \tag{F9}$$

(where ξ and τ should not be confused with those of same name in Appendix C), the master equation (F4) becomes dimensionless and contains no free parameters,

$$\partial_\tau \tilde{n}(\xi,\tau) = \partial_\xi \tilde{n}(\xi,\tau) - \xi \tilde{n}(\xi,\tau) + 2\int_\xi^\infty d\xi' \tilde{n}(\xi',\tau). \tag{F10}$$

From the master equation follow equations for the total length of tubulin-t, $\chi(t)$, and the total number of patches $n(t)$ per unit length of microtubule

$$\frac{d}{dt}\chi(t) = -w_h n(t) \tag{F11}$$

and

$$\frac{d}{dt}n(t) = -w_h n(0,t) + r\chi(t). \tag{F12}$$

The interpretation of these coupled equations is obvious, but they do not close because $n(0,t)$ occurs. Only the master equation closes. It has the solution

$$\tilde{n}(\xi,\tau) = \tau^2 \exp(-\tau\xi - \tau^2/2) \tag{F13}$$

or, returning to variables x, t, and $n(x,t)$,

$$n(x,t) = (rt)^2 \exp(-rtx - rw_h t^2/2) \tag{F14}$$

and, consequently,

$$n(t) = rt\exp(-rw_h t^2/2), \tag{F15}$$

$$\chi(t) = \exp(-rw_h t^2/2). \tag{F16}$$

The form of the solution $n(x,t)$ in Eq. (F14) is easily understood. Internal hydrolysis of the infinite microtubule is a Poisson process causing an exponential distribution of patch lengths x. This Poisson process is superposed with the shrinking at velocity w_h of the patches it creates. But an exponential distribution on the positive half axis remains invariant under a shift of the origin of the axis. So the shrinking process does not change the character of the result of the Poisson process. Were it not for the shrinking and vanishing of patches, the Poisson process would have resulted in a density rt of points of internal hydrolysis, hence in $n(t) = rt$ patches per unit length, with average length

$$\langle x \rangle = 1/(rt),$$

from which

$$n(x,t) = (rt)^2 \exp(-rtx)$$

follows because patches shrink and vanish, their number does not just grow as rt. But the patches present at any time t are, nevertheless, distributed in x according to the distribution just given. So the shrinking process does not affect the distribution of patch lengths. Only the *number* of patches is affected: compare Eqs. (F14) and (F15) with the same expressions for $w_h = 0$.

APPENDIX G: GTP HYDROLYSIS RATES—CASE OF MICROTUBULES GROWING AT DECREASING RATE

In Sec. VIII C we considered the case of GTP hydrolysis of caps grown with constant microtubule growth rate v_g. If instead v_g *decreases* as the microtubules grow, because the concentration of tubulin-t in solution is depleted by their growth, the situation is more complicated. Depletion of tubulin-t takes place in the hydrolysis experiments reported in [17], [43], and [40]. So for the benefit of the reader wanting more than the upper bound given in Sec. VIII C, we present our model's predictions in this appendix.

If the characteristic time for depletion is much longer than the characteristic time for hydrolysis t_h, we have a quasistationary growth rate as regards hydrolysis and the hydrolysis rate and the amount of tubulin-t present at microtubule ends will follow the instantaneous growth rate; the results in Sec. VIII C apply when the instantaneous growth rate is substituted for the constant groat rate assumed there.

This is not the situation in the experiments described in [17] and [43]. In those experiments tubulin-*t* depletion occurred at rates comparable to t_h. This appendix describes that situation.

When stabilized microtubules grow with a velocity v_g that is proportional to the tubulin-t concentration c,

$$v_g = v_g' c, \tag{G1}$$

and deplete the latter by their growth, the absence of catastrophes makes them all grow to the same length $l(\infty)$ and in the same way

$$l(t) = l(\infty)(1 - e^{-\nu_{\mathrm{MT}} v_g' t}) = l(\infty)(1 - e^{-t/t_d}), \tag{G2}$$

where we have introduced the characteristic time

$$t_d = \frac{1}{\nu_{\mathrm{MT}} v_g'} \tag{G3}$$

for depletion of the tubulin-t concentration by a constant concentration of microtubules ν_{MT}. The assumption that the concentration of microtubules is constant during their growth applies in the experiment described in [17] because microtubules are grown from seeds; see [18], Fig. 1. When microtubules are nucleated in the bulk of the tubulin-t solution, the randomness of the nucleation process gives rise to a distribution of finite width for the lengths of microtubules at any given time, compare [43], Fig. 4(E). In this case Eq. (G2) applies only to the distributions average length and only after nucleation has been effectively stopped by depletion of tubulin-t.

At time t, the *age since assembly* t' of the part of the microtubule located a distance l' behind its growing tip satisfies the equation

$$l(t - t') = l(t) - l'. \tag{G4}$$

Using this with Eqs. (G2) and (F16), we find for the total amount of GTP present at time t,

$$
\begin{aligned}
l_{\mathrm{GTP}}(t) &= \int_0^{l(t)} dl' \chi[t'(l')] \\
&= l(\infty) e^{-t/t_d} t_d^{-1} \int_0^t dt' e^{t'/t_d} \chi(t') \\
&= l(\infty) \sqrt{\frac{\pi}{2}} \frac{t_h}{t_d} e^{(t_h/t_d)^2/2} e^{-t/t_d} \\
&\quad \times \left[\mathrm{sgn}\left(\frac{t}{t_h} - \frac{t_h}{t_d} \right) \Phi\left(\frac{t}{\sqrt{2} t_h} - \frac{t_h}{\sqrt{2} t_d} \right) + \Phi\left(\frac{t_h}{\sqrt{2} t_d} \right) \right] \\
&\sim l(\infty) \sqrt{\frac{\pi}{2}} \frac{t_h}{t_d} e^{(t_h/t_d)^2/2} e^{-t/t_d} \left[1 + \Phi\left(\frac{t_h}{\sqrt{2} t_d} \right) \right], \quad \text{(G5)}
\end{aligned}
$$

where the last expression gives the asymptotic behavior at late times t.

The GTP content of a microtubule described by this result has a maximum at a time that can be determined from the expression given. But as shown in Sec. VIII C, bounds can easily be established, which suffice to understand the key experimental result, the zero result in [17], and we give Eq. (G5) only to show it can be found within our approach, to put it on record for anybody wanting a description taking depletion into account, and to illustrate the complexity of such a description.

In the experiments described in [17] and [43], the GTP content of microtubules is not measured directly. The total amount of microtubule $l(t)$ is measured both turbidimetrically and by radioactive labeling and the total amount of GDP produced is measured by radioactive labeling of the phosphate ion released in the hydrolysis of GTP to GDP. Since the microtubules polymerized in those experiments are stabilized against depolymerization, the GDP produced is all located in microtubules and

$$
\begin{aligned}
l_{\mathrm{GDP}}(t) &= l(t) - l_{\mathrm{GTP}}(t) \\
&= l(\infty) \left(1 - \left\{ 1 + \sqrt{\frac{\pi}{2}} \frac{t_h}{t_d} e^{(t_h/t_d)^2/2} \right. \right. \\
&\quad \times \left[\mathrm{sgn}\left(\frac{t}{t_h} - \frac{t_h}{t_d} \right) \Phi\left(\frac{t}{\sqrt{2} t_h} - \frac{t_h}{\sqrt{2} t_d} \right) \right. \\
&\quad \left. \left. \left. + \Phi\left(\frac{t_h}{\sqrt{2} t_d} \right) \right] \right\} e^{-t/t_d} \right) \quad \text{(G6)} \\
&\sim l(\infty) \left(1 - \left\{ 1 + \frac{t_h}{t_d} \sqrt{\frac{\pi}{2}} e^{(t_h/t_d)^2/2} \right. \right. \\
&\quad \left. \left. \times \left[1 + \Phi\left(\frac{t_h}{\sqrt{2} t_d} \right) \right] \right\} e^{-t/t_d} \right), \quad \text{(G7)}
\end{aligned}
$$

where the last expression gives the asymptotic behavior at late times t.

[1] T. Mitchison and M. Kirschner, Nature **312**, 232 (1984).
[2] T. Mitchison and M. Kirschner, Nature **312**, 237 (1984).
[3] M.-F. Carlier and D. Pantaloni, Biochemistry **20**, 1918 (1981).
[4] H. P. Erickson and E. T. O'Brien, Annu. Rev. Biophys. Biomol. Struct. **21**, 145 (1992).
[5] M. Caplow, Curr. Opinion Cell Biol, **4**, 58 (1992).
[6] M.-F. Carlier, Int. Rev. Cytol. **115**, 139 (1989).
[7] Graphics are by Imre Janosi.
[8] R. H. Wade and D. Chrétien, J. Struct. Biol. **110**, 1 (1993).
[9] M. Maaloum, D. Chrétien, E. Karsenti, and J. K. H. Horber, J. Cell Sci. **107**, 3127 (1994).
[10] D. Kuchnir Fygenson, E. Braun, and A. Libchaber, Phys. Rev. E **50**, 1579 (1994).
[11] S. R. Martin, M. J. Schilstra, and P. M. Bayley, Biophys. J. **65**, 578 (1993).
[12] Y. Chen and T. L. Hill, Proc. Natl. Acad. Sci. U.S.A. **82**, 1131 (1985).
[13] D. N. Drechsel, A. A. Hyman, M. H. Cobb, and M. W. Kirschner, Mol. Biol. Cell **3**, 1141 (1992).
[14] R. A. Walker, E. T. O'Brien, N. K. Pryer, M. F. Soboeiro, W. A. Voter, and H. P. Erickson, J. Cell Biol. **107**, 1437 (1988).
[15] W. A. Voter, E. T. O'Brien, and H. P. Erickson, Cell Motil. Cytoskel. **18**, 55 (1991).
[16] R. A. Walker, N. K. Pryer, and E. D. Salmon, J. Cell Biol. **114**, 73 (1991).
[17] R. J. Stewart, K. W. Farrell, and L. Wilson, Biochemistry **29**, 6489 (1990).
[18] D. J. Odde, L. Cassimeris, and H. M. Buettner, Biophys. J. **69**, 796 (1995).
[19] D. D. Drechsel and M. W. Kirschner, Curr. Biol. **4**, 1053 (1994).
[20] R. A. Walker, S. Inoué, and E. D. Salmon, J. Cell. Biol. **108**, 931 (1989).
[21] H. Flyvbjerg, T. E. Holy, and S. Leibler, Phys. Rev. Lett. **73** 2372 (1994).
[22] P. M. Bayley, M. J. Schilstra, and S. R. Martin, J. Cell Sci. **95**, 33 (1990).
[23] The result reported in [13] may, of course, depend on the buffer used as well as other experimental conditions. However, the model we derive here under the assumption of a zero off rate covers the case of a nonzero off rate as well, in the sense that the resulting mesoscopic model is the same when expressed in terms of its parameters r and D and its variable v. However, its interpretation in terms of underlying processes has changed, of course.
[24] Specifically, Eq. (6) is no longer valid, but replaced by $2D = (k_g + k_g^{(\mathrm{off})} + k_h)\,\delta x^2$, where $k_g^{(\mathrm{off})}$ is the off rate complementing the on rate k_g. In the case where the off rate is not known from direct experimental measurement, the net result is a theory with one more free, though necessarily positive, parameter to be determined by fitting the theoretical catastrophe rates and waiting times upon dilution derived here to experimental data. With the data we fit to, a positive off rate gives better fits than those we show. But we already know from [13]

that the rate is zero with rather good experimental precision, hence we can work with one less parameter to fit and consequently obtain a correspondingly stronger test of the model.

[25] In general, experiments testing the model are optimized by including direct measurements of the off rate in addition to measurements of the catastrophe rate and the waiting time upon dilution and all experiments should be done with the same preparation of tubulin and in the same buffer.

[26] M. Caplow, R. Ruhlen, J. Shanks, R. A. Walker, and E. D. Salmon, Biochemistry **28**, 8136 (1989).

[27] F. Verde, M. Dogterom, E. Stelzer, E. Karsenti, and S. Leibler, J. Cell Biol. **118**, 1097 (1992).

[28] N. R. Gliksman, S. F. Parsons, and E. D. Salmon, J. Cell Biol. **119**, 1271 (1992).

[29] K. R. Summers and M. W. Kirschner, J. Cell Biol. **83**, 205 (1979).

[30] T. Horio and H. Hotani, Nature **321**, 605 (1986).

[31] E. T. O'Brien, E. D. Salmon, R. A. Walker, and H. P. Erickson, Biochemistry **29**, 6648 (1990).

[32] This follows upon setting v_g- (before dilution) $\gg v_h$ and v_g (after dilution) $=0$. This second condition deserves some clarification. One does not expect dilution to be complete. In fact, the authors [16] estimate that the tubulin concentration after dilution is as high as 3 μM. However, with their conditions this is probably not sufficient to generate any growth; in fact, one might expect that the microtubule should shrink slowly, even without suffering a catastrophe [14]. However, the growth rate at these low tubulin concentrations is controversial and almost certainly dependent on conditions [13], so we make the simplest reasonable assumption and set v_g, (after dilution) $=0$.

[33] M. Caplow, R. L. Ruhlen, and J. Shanks, J. Cell. Biol. **127**, 779 (1994).

[34] J. R. Simon, S. F. Parsons, and E. D. Salmon, Cell Motil. Cytoskel. **21**, 1 (1992).

[35] M. J. Schilstra, P. M. Bayley, and S. R. Martin, Biochem. J. **277**, 839 (1991).

[36] In theory, the combined fit shown here to the plus-end catastrophe rate and the plus-end delay time for dilution-induced catastrophes does not involve the minus-end data. In practice it does, because we also fit an effective time of dilution because dilution was initiated at $t=0$ and required some time for completion. This last parameter is the same for the plus- and minus-end data, we can reasonably assume, since they were taken with the same apparatus. For this practical reason, the fitting to plus-end data are not done separately, but as a combined fit to plus- and minus-end data.

[37] M. F. Carlier, T. L. Hill, and Y. Chen, Proc. Natl. Acad. Sci. U.S.A. **81**, 771 (1984).

[38] E. Hamel, J. K. Batra, A. B. Huang, and C. M. Lin, Arch. Biochem. Biophys. **245**, 316 (1986).

[39] Maria J. Schilstra, Stephen R. Martin, and Peter M. Bayley, Biochem. Biophys. Res. Commun. **147**, 588 (1987).

[40] E. T. O'Brien, W. A. Voter, and H. P. Erickson, Biochemistry **26**, 4148 (1987).

[41] M.-F. Carlier, D. Didry, and D. Pantaloni, Biochemistry **26**, 4428 (1987).

[42] R. J. Stewart, K. W. Farrell, and L. Wilson, J. Cell Biol. **107**, 241a (1988).

[43] R. Melki, M.-F. Carlier, and D. Pantaloni, Biochemistry **29**, 8921 (1990).

[44] M. F. Carlier. Mol. Cell. Biochem. **47**, 97 (1982).

[45] T. L. Hill and M.-F. Carlier, Proc. Natl. Acad. Sci. U.S.A. **80**, 7234 (1983).

[46] T. L. Hill and Y. Chen, Proc. Natl. Acad. Sci. U.S.A. **81**, 5772 (1984).

[47] M. Caplow and R. Reid, Proc. Natl. Acad. Sci. U.S.A **82**, 3267 (1985).

[48] P. M. Bayley, M. J. Schilstra, and S. R. Martin, J. Cell Sci. **93**, 241 (1989).

[49] P. M. Bayley, M. J. Schilstra, and S. R. Martin, J. Cell Sci. **95**, 329 (1990).

[50] R. K. McNeal and D. L. Purich, J. Biol. Chem. **253**, 4683 (1978).

[51] E. Hamel, A. A. del Campo, M. C. Lowe, P. G. Waxman, and C. M. Lin, Biochemistry **21**, 503 (1982).

[52] D. Chrétien, S. D. Fuller, and E. Karsenti, J. Cell Biol. **129**, 1311 (1995).

[53] R. C. Weisenberg, Science **177**, 1104 (1972).

[54] J. B. Olmsted and G. G. Borisy, Biochemistry **14**, 2996 (1975).

[55] R. P. Frigon and S. N. Timasheff, Biochemistry **14**, 4567 (1975).

[56] J. C. Lee and S. N. Timasheff, Biochemistry **16**, 754 (1977).

[57] V. Gal, S. Martin, and P. Bayley, Biochem. Biophys. Res. Commun. **102**, 1464 (1988).

[58] E. T. O'Brien, R. A. Walker, E. D. Salmon, and H. P. Erickson, in *Cytoskeletal and Extracellular Proteins*, edited by U. Aebi and J. Engel (Springer-Verlag, Berlin, 1989), pp. 259–261.

[59] D. L. Gard and M. W. Kirschner, J. Cell Biol. **105**, 2203 (1987).

[60] R. J. Vasquez, D. L. Gard, and L. Cassimeris, J. Cell Biol. **127**, 985 (1994).

[61] S. S. L. Andersen, B. Buendia, J. E. Dominguez, A. Sawyer, and E. Karsenti, J. Cell Biol. **127**, 1289 (1994).

[62] M. Dogterom, M. A. Felix, C. C. Guet, and S. Leibler, J. Cell Biol. **133**, 125 (1996).

[63] R. A. Walker, University of North Carolina Ph.D. thesis, Chapel Hill, 1989 (unpublished).

[64] C. E. Walczak, T. J. Mitchison, and A. Desai, Cell **84**, 37 (1996).

[65] E. D. Salmon, Science **189**, 884 (1975).

[66] B. Bourns, S. Franklin, L. Cassimeris, and E. D. Salmon, Cell Motil. Cytoskel. **10**, 380 (1988).

[67] E. D. Salmon (private communication).

[68] R. F. Gildersleeve, A. R. Cross, K. E. Cullen, A. P. Fagen, and R. C. Williams, J. Biol. Chem. **267**, 7995 (1992).

[69] *Handbook of Mathematical Functions*, edited by M. Abramowitz and I. A. Stegun (Dover, New York, 1972).